Atmospheric Research 304 (2024) 107396

Contents lists available at ScienceDirect

Atmospheric Research

journal homepage: www.elsevier.com/locate/atmosres

Direct radiative forcing of light-absorbing carbonaceous aerosols in China

Liu Yang [a], Yuhao Mao [a,b,*], Hong Liao [a,b], Mingjie Xie [a], Ying Zhang [c]

[a] Jiangsu Key Laboratory of Atmospheric Environment Monitoring and Pollution Control/Jiangsu Collaborative Innovation Center of Atmospheric Environment and Equipment Technology, School of Environmental Science and Engineering, Nanjing University of Information Science and Technology (NUIST), Nanjing 210044, China
[b] Key Laboratory of Meteorological Disaster, Ministry of Education (KLME)/Collaborative Innovation Center on Forecast and Evaluation of Meteorological Disasters (CIC-FEMD)/International Joint Research Laboratory on Climate and Environment Change (ILCEC), NUIST, Nanjing 210044, China
[c] State Environmental Protection Key Laboratory of Satellite Remote Sensing, Institute of Remote Sensing and Digital Earth, Chinese Academy of Sciences, Beijing 100101, China

ARTICLE INFO

Keywords:
Light-absorbing carbonaceous aerosols
Direct radiative forcing
Absorption aerosol optical depth

ABSTRACT

China is an important emitter of light-absorbing carbonaceous aerosols (LACs), including black carbon (BC) and brown carbon (BrC). Currently, there are large uncertainties in model-estimated direct radiative forcing (DRF) of LACs, partially due to the poor understanding of the emissions and optical properties of LACs. In this study, we estimated the DRF of LACs over China during the implementation of the Air Pollution Prevention and Control Action Plan (APPCAP) using the global chemical transport model (GEOS-Chem) coupled with the Rapid Radiative Transfer Model of GCMs (RRTMG). We updated the refractive index of BC, includedbiomass burning (BB) sources, biofuel (BF) and coal combustion (CC) sources in the residential sector as BrC emission sources and the optical properties were updated, which were not fully considered in the previous model studies. Our results showed that model could reasonably capture the spatial and temporal variations of LACs in China with the correlation coefficients between model simulated and Aerosol Robotic Network (AERONET) observed daily absorption aerosol optical depth (AAOD) of LACs at 440 nm above 0.63 and the corresponding values of the normalized mean bias within ±30%. The simulated annual mean LACs AAOD at 440 nm in China was 0.016 (0.021) in 2017 (2014) and BrC contributed about 20% (21%). The estimated annual mean clear-sky LACs DRF at the top of the atmosphere in China was 1.02 W m^{-2} in 2017 and 1.38 W m^{-2} in 2014, and the contribution of BrC was about 10% and 11%, respectively, which was dominated by the BF sources (46% in 2017 and 44% in 2014) and the BB sources (38% in 2017 and 43% in 2014), with CC sources being low (16% in 2017 and 13% in 2014). The annual mean AAOD and DRF of LACs in China decreased by 0.005 and 0.36 W m^{-2} from 2014 to 2017, which were largely attributed to the reductions of anthropogenic emissions during the implementation of APPCAP. Our results would improve the understanding of the light absorption capacity and climate effects of LACs in China.

1. Introduction

Light-absorbing carbonaceous aerosols (LACs), including black carbon (BC) and brown carbon (BrC), can affect the cloud formation, reduce the ice/snow albedo, and introduce positive radiative forcing (RF), which has a significant impact on the Earth's climate system (Bond et al., 2013; Bhat et al., 2017; Yan et al., 2018). BC is a black particle produced in the flame stage of fuel combustion with strong absorption and weak spectral dependence in the visible region (Patterson and McMahon, 1984), which plays an important role in climate change (Liu et al., 2020a). BrC is a weakly absorbing but wavelength-dependent brown particle produced in the smolder stage (Patterson and McMahon, 1984; Saleh, 2020; Sun et al., 2021), and is likewise a light-absorbing fraction of organic carbon (OC) or organic aerosols (OA) with a strong absorption in the near ultraviolet (UV) spectral region (Andreae and Gelencser, 2006). The light absorption by BrC typically accounts for 20–40% of the total global absorption of carbonaceous aerosols (Jo et al., 2016; Park et al., 2010; Saleh et al., 2014; Wang et al., 2018a).

With the accelerated urbanization and rapid economic development, China becomes one of the countries with the high emissions of LACs. Previous studies have shown that BC emissions in China accounted for about 25% of the total global BC emissions (Bond et al., 2007; Wang

* Corresponding author at: School of Environmental Science and Engineering, Nanjing University of Information Science and Technology (NUIST), Nanjing 210044, China.
E-mail address: yhmao@nuist.edu.cn (Y. Mao).

https://doi.org/10.1016/j.atmosres.2024.107396
Received 16 December 2023; Received in revised form 26 March 2024; Accepted 2 April 2024
Available online 9 April 2024

et al., 2012) and BrC emissions in China (1.5 Tg) (Wang et al., 2022a) might be close to BC emissions (1.3 Tg) in 2017 (Zheng et al., 2018). Observational studies (Cheng et al., 2011, 2016; Liu et al., 2018a; Mo et al., 2021) have shown that BC (BrC) concentrations in northern China could reach up to 35 (16) μg m^{-3} in 2015 (2014). In addition, observed mass absorption efficiency (MAE) of BrC was as high as 1.9 m^2/gC at 365 nm in 2014 in Northwest China, 1.8 m^2/gC in North China and 1.7 m^2/gC in Yangtze River Delta (Mo et al., 2021; Xie et al., 2020), which likely resulted from the low combustion efficiencies of BrC sources from open biomass burning and residential solid fuels in China (Sun et al., 2021; Wang et al., 2012). The observed light absorption coefficients of BrC in China were also high, e.g., 10–15 M m^{-1} in Beijing in 2014 (Cheng et al., 2016, 2011; Mo et al., 2021), 13 M m^{-1} in Changchun in 2017 (Meng et al., 2020) and 22 M m^{-1} in Sanjiang Plain in 2013 (Zhai et al., 2019).

Numerous studies have shown that large uncertainties are existed in the estimating the direct radiative forcing (DRF) of LACs (Tuccella et al., 2020; Wang et al., 2014, 2018a). For BC, model-based studies have shown that BC DRF at the top of the atmosphere (TOA) was in the range of 0.81–2.20 W m^{-2} in China (Li et al., 2016; Mao et al., 2016; Yang et al., 2017; Zhuang et al., 2013), which was higher than the global mean BC DRF of 0.39–0.71 W m^{-2} (Bond et al., 2013; Zhang et al., 2020a). The estimate of BC DRF depends on the BC concentration as well as the BC optical properties, which are significantly affected by refractive index (Bond and Bergstrom, 2006; Liu et al., 2020b; Wang et al., 2014), particle structures/morphology (Liu and Mishchenko, 2018; He, 2019), size distribution of particle (Wang et al., 2014; Zheng and Wu, 2021), aging and coating processes (Luo et al., 2019; Tan et al., 2020), etc. For BrC, due to the limitations of the emission inventory and the inconsistency of optical properties (Saleh et al., 2014; Wang et al., 2022a), simulated BrC DRF at TOA is in a wide range of 0.05–0.57 W m^{-2} globally (Feng et al., 2013; Lin et al., 2014; Wang et al., 2014; Zhang et al., 2020a).

The refractive index of BC has great influence on its optical properties (Cappa et al., 2012; Feng et al., 2021; Wang et al., 2014). Bond et al. (2013) mentioned that the uncertainty of MAE due to refractive index could reach 30% if other factors remained consistent. Previous studies (Sand et al., 2021; Wang et al., 2014; Wang et al., 2018a; Zhang et al., 2021a) have shown that the commonly default BC refractive indices in the model, such as 1.75 + 0.44i and 1.85 + 0.71i, couldn't represent the observations well. Liu et al. (2020b) also showed that the updated and widely used refractive index of 1.95 + 0.79i still couldn't most accurately represent the true refractive index of BC.

Previous modeling studies of BrC generally only considered biofuels (BF) and biomass burning (BB) as the sources of light absorption. Observational studies have indicated that BrC from fossil fuel combustion sources was also light-absorbing (Xie et al., 2017; Yan et al., 2017). However, fossil fuel was not generally included in the model simulations of BrC DRF because emissions had not been fully characterized (Wang et al., 2018a). Recent studies have shown that residential coal combustion (CC) in China was a significant source of BrC (Huang et al., 2022; Tang et al., 2020a; Wang et al., 2020). Wang et al. (2022a) estimated that BrC emissions from CC in the residential sector accounted for 25%–30% of the total BrC emissions in China from 2000 to 2020. It is thus necessary to consider residential CC to improve the understanding of the climate effects of BrC.

Since 2013, Chinese government implemented the Air Pollution Prevention and Control Action Plan (APPCAP, http://www.gov.cn/zhengce/content/2013-09/13/content_4561.htm), and the annual mean $PM_{2.5}$ (particulate matters with aerodynamic diameter < 2.5 μm) concentrations in the three metropolitan areas in eastern China decreased by 28–40% within five years (Zhang et al., 2017; Liu et al., 2016; Zhao et al., 2017). To our knowledge, few studies have systematically investigated the absorption aerosol optical depth (AAOD) and DRF of LACs from multiple combustion sources in China during the implementation of APPCAP. In this study, we use the global chemical transport model GEOS-Chem coupled with the Rapid Radiative Transfer Model of the GCM (RRTMG) to quantify the AAOD and DRF of BC and BrC in China in 2014 and 2017. We update the refractive index of BC, include BB emissions and residential CC and BF as the main sources of BrC and assign corresponding optical properties to different sources. Section 2 presents the model description, numerical experiments, and observational datasets. Section 3 and 4 includes model simulated BC (OC) concentrations and LACs AAOD as well as model evaluations based on observations. Sections 5 shows the model-estimated radiative forcing of LACs. Finally, Sections 6 and 7 discuss the uncertainties and conclusions.

2. Data and methods

2.1. The GEOS-Chem Model

The GEOS-Chem model is a global three-dimensional atmospheric chemical transport model (http://geos-chem.org) managed by Harvard University, USA, supported by an open-source community of all users, and driven by the meteorological field provided by the National Aeronautics and Space Administration (NASA) Global Modeling and Assimilation Office (GMAO). The present study uses the GEOS-Chem-RRTMG model (version 12.0) to simulate the LACs DRF for instantaneous shortwave and longwave radiation fluxes every 3 h (Wang et al., 2014). The model is driven by Modern-Era Retrospective Analysis for Research and Applications, Version 2 (MERRA2) assimilated meteorological data from NASA's Goddard Earth Observing System (GEOS) at the horizontal resolution of 2° × 2.5° and with 47 vertical layers from the surface to 0.01 hPa.

The simulation of carbonaceous aerosols in the GEOS-Chem model is followed by Park, 2003, which assumes that 80% of BC and 50% of primary OC are hydrophobic in nature when discharged and become hydrophobic with the e-folding time of 1.15 days (Park, 2005). Previous studies have shown that assuming this fixed aging time can result in large uncertainties particularly over source regions like China (Chen et al., 2017; He et al., 2016). Wet deposition of aerosols is calculated as described by Liu et al. (2003) and updated by Wang et al. (2011), including the removal from convective updrafts, convective anvils, and large-scale precipitation within the cloud and below the cloud. Dry deposition of aerosols uses the series resistance model by Walcek et al. (1986), depending on local surface type and meteorological conditions.

According to Wang et al. (2014), the BC dry particles are spherical and the density of BC is updated to 1.8 g/cm^3. The refractive index is related to the type of aerosol species and varies with different chemical properties (Ma et al., 2012). Previous study (Liu et al., 2020b) has shown that both the default refractive index of BC at 550 nm (1.75 + 0.44i) and that recommended by Bond et al. (2006) (1.95 + 0.79i) may underestimate the absorption of BC. Based on the studies of Schnaiter, 2005 and Liu et al. (2020b), we use the refractive index of BC at 550 nm by 1.90 + 1.0i in the present study. In addition, the enhanced BC absorption induced by the coating is included by multiplying a scaling factor of 1.5 (Wang et al., 2014; Zhang et al., 2021a).

The Harvard-NASA Emission Control (HEMCO) is used in the GEOS-Chem model to treat the emission of atmospheric pollutants. The global anthropogenic emissions are from Emissions Database for Global Atmospheric Research (EDGARv4.3, http://wiki.seas.harvard.edu/geos-chem/index.php/EDGAR_v4.3_anthropogenic_emissions) for 2010. Monthly anthropogenic emissions (BC, OC, SO_2, CO, VOCs, NO_x, NH_3) in China are derived from multi-resolution emission inventories (MEICv1.3) of China for 2014 and 2017, including residential, industrial, transportation, power, and agricultural emission sectors, and weekly and daily variations of the emissions are considered by using daily and hourly scaling factors, the impact of the APPCP has been taken into account in emissions (Zheng et al., 2018). Biogenic emissions of VOCs are calculated by the Model of Emissions of Gases and Aerosols from Nature (MEGAN) version 2.1 with updates from Guenther et al.

(2012). Open biomass burning emissions are from the fourth version of the Global Fire Emission Database Inventory (GFEDv4) for 2014 and 2017, with a monthly temporal resolution (van der Werf et al., 2017).

2.2. Treatment of BrC

In the current version of coupled GEOS-Chem-RRTMG model, the emission inventory of BrC is not available, and only the BC and OC emission are included for the simulations of carbonaceous aerosols, and the DRF of BC and OA are simulated. In the default setting of GEOS-Chem model, the concentrations of POA are calculated from POC based on an OA/OC ratio of 2.1 (Wang et al., 2018a). To study the BrC AAOD and DRF, we thus refer to the study of Wang et al. (2018a) to re-assigned optical properties to OA, which has low-light absorption capacity as it contains light-absorbing BrC.

The main sources of BrC aerosols in China are open-air BB and residential solid fuel combustion (both BF and CC) (Li et al., 2019; Zhang et al., 2021b). Observational studies have shown that the MAE of BrC is related to the type of combustion source, and combustion conditions (e.g., Akagi et al., 2011; Chen and Bond, 2010; Saleh et al., 2014). Saleh et al. (2014) showed that the effective OA absorption (the imaginary part of the refractive index, k_{OA}) of BF and BB sources was positively correlated with the emission ratios of BC to OA. However, there are no studies showing correlation between MAE and BC/OC emission ratios for fossil fuel combustion sources (e.g., Saleh et al., 2014; Xie et al., 2018; Xie et al., 2017). We thus used BC/OA ratios to parameterize the k_{OA} only for BF and BB sources, and the refractive index of OA (RI_{OA}) is shown in eq. (1):

$$RI_{OA} = 1.53 + \left(0.016 \bullet log_{10}\left(\frac{BC}{OA}\right) + 0.04\right) \bullet \left(\frac{550}{\lambda}\right)^{\omega} i \quad (1)$$

$$\omega = \frac{0.21}{\frac{BC}{OA} + 0.07} \quad (2)$$

where the real part (1.53) is commonly used in previous studies (Chen and Bond, 2010; Drugé et al., 2022; Lin et al., 2014; Tuccella et al., 2020), and the imaginary part at 550 nm is taken from the results of Saleh et al. (2014). Eq. (2) then represents the dependence of k_{OA} on wavelength. According to the previous studies (Shen et al., 2013; Tian et al., 2017; Zhang et al., 2021b), the BC/OC emission ratio from BF in China ranges from 0.073 to 0.42, and we use the mean value of 0.246 for BC/OC in China and the corresponding value of 0.117 for BC/OA. For open biomass burning sources from the GFEDv4 inventory, the average BC/OA emission ratio of 0.05 in China is used in this study.

For the optical properties of BrC emitted from CC sources in the residential sector, we use the direct assignment of the observed MAE_{OA}. At present, the measurements of the optical absorption properties of BrC are mainly based on the chemical method and the optical method (Yuan et al., 2022). Chemical methods, also known as extraction methods, involve solvent extraction of collected samples followed by UV–visible spectroscopic analysis of the extracts (Chen and Bond, 2010; Cheng et al., 2017). Wang et al. (2022a) showed that chemical methods are highly uncertain due to a series of differences in extraction solvent, BrC properties to be extracted, solution absorption and aerosol absorption conversion. Therefore, the MAE used for model simulation in this study are from measurement by optical methods to provide a consistent estimate of the absorption of BrC. Based on the study of Yuan et al. (2022), we use MAE_{OC} with a value of 1.9 $m^2\ g^{-1}$ at 405 nm for CC in the residential sector (AAE = 3.7, Ångström exponent) and a resulting MAE_{CCOA} of 0.90 $m^2\ g^{-1}$. The MAE values for other wavelengths are calculated using the following functions (Bond and Bergstrom, 2006):

$$MAE(\lambda) = MAE(\lambda_0) \cdot \left(\frac{\lambda_0}{\lambda}\right)^{AAE} \quad MAE\lambda = MAE\lambda 0^{*}(\lambda 0\lambda)AAE \quad (3)$$

where λ_0 is 405 nm for MAE_{CCOA}. The imaginary part of the OA refractive index ($k_{OA,\lambda}$) is estimated using the following equation (Liu et al., 2013):

$$k_{OA,\lambda} = \frac{MAE(\lambda)\rho\lambda}{4\pi} \quad (4)$$

where ρ is the density of OA (g cm^{-3}) and the default value of 1.3 g cm^{-3} is used in GEOS-Chem. For BrC, we update the $k_{OA,\lambda}$ in the 300-600 nm range, as there is less absorption of BrC in other longer bands.

Since the residential emissions used in the present study are not classified into CC and BF sources, we use observed BC/OC emission ratios of the two sources to separate the CC and BF sources in the residential sector (Novakov et al., 2000; Zhang et al., 2021b). The BC/OC emission ratio from CC source in residential sector ranges from 0.02 to 1.47 in China (Shen et al., 2013; Tian et al., 2017; Zhang et al., 2021b; Zhi et al., 2008), and we use the mean value of 0.745. We then use the observed BC/OC emission ratio from the two sources and model simulated BC/OC column concentration ratio from the residential sector at each model grid to separate the contribution of CC and BF to OA AAOD and DRF in the residential sector.

2.3. Numerical experiments

In this study, the LACs DRF is simulated in 2014 and 2017 based on the GEOS-Chem-RRTMG model driven by the MERRA-2 meteorological field. According to the parameterization of k_{OA} for different BrC sources mentioned above, the following numerical experiments are set up in this study (Table 1). All simulations are preceded by a one-month spin-up. Absorption from biogenic sources (Lin et al., 2014; Saleh et al., 2015) and aromatic sources of secondary organic aerosols (SOA) (Wang et al., 2014; Jo et al., 2016; Wang et al., 2018) are not included in this study, which would lead to an underestimation of BrC DRF, although studies have shown that the light absorption from BrC primary emissions is significantly greater than that from secondary processes (Martinsson et al., 2015; Saleh et al., 2013; Wang et al., 2016).

1.CTRL: Standard simulation to quantify the BC and OA AAOD and DRF in China, BC with updated complex refractive index and OA with default optical properties, as well as anthropogenic and open biomass burning emissions are included

2.no_RES: Same as the CTRL simulation except that BC and OC emissions from residential sector in China are set to zero.

3.no_GFEDv4: Same as the CTRL simulation except that BC and OC emissions from biomass burning are set to zero.

4. ALL_BF: Same as the CTRL simulation except that the the default k_{OA} for OA is updated to k_{BFOA}

5. no_RES_BF: Same as the ALL_BF simulation except that OC emissions from residential sector in China are set to zero.

6. ALL_BB: Same as the CTRL simulation except that the default k_{OA} for OA is updated to k_{BBOA}

7. no_GFEDv4_BB: Same as the ALL_BB simulation except that OC emissions from biomass burning are set to zero.

Table 1
GEOS-Chem simulations of LACs.

Model experiments	k_{OA}	OC emissions[a]	
		Anthropogenic	Open biomass burning
CTRL	Default value	√	√
no_RES	Default value	no Residential	√
no_GFEDv4	Default value	√	no GFEDv4
ALL_BF	k_{BFOA}	√	√
no_RES_BF	k_{BFOA}	no Residential	√
ALL_BB	k_{BBOA}	√	√
no_GFEDv4_BB	k_{BBOA}	√	no GFEDv4
ALL_CC	k_{CCOA}	√	√
no_RES_CC	k_{CCOA}	no Residential	√

[a] BC emissions from different anthropogenic and natural sources are also included.

8. ALL_CC: Same as the CTRL emulation except that the default k_{OA} for OA is updated to k_{CCOA}

9. no_RES_CC: Same as the ALL_CC simulation except that OC emissions from residential sector in China are set to zero.

According to the method described in Section 2.2, the BrC AAOD and DRF of the BF and CC sources in the residential sector are quantified by ((ALL_BF - no_RES_BF) - (CTRL - no_RES)) and ((ALL_CC - no_RES_CC) - (CTRL - no_RES)), and the BrC AAOD and DRF of the BB sources are quantified by ((ALL_ BB - no_GFEDv4_BB)- (CTRL - no_GFEDv4)).

2.4. Observations

2.4.1. BC and OC concentrations

Previous studies (Li et al., 2016; Mao et al., 2016, 2020) have shown that the GEOS-Chem model can reasonably capture spatial and temporal variations of aerosol concentrations in China. We further evaluate the ability of the GEOS-Chem model to simulate diurnal variations of BC concentration in China by using ground-based measurements from two sites: Xianghe (39.80°N, 116.96°E, 36 m) for 2014 (Mao et al., 2020) and Nanjing Caochangmen (32.06°N, 118.75°E, ~20 m) for 2017 (Xie et al., 2022; Yu et al., 2020), where the Nanjing Caochangmen site is also used to assess simulated OC concentration. The observed surface BC (OC) concentrations obtained from the literatures are listed in Table 2, which includes the seasonal and annual mean surface BC (OC) concentrations measured at 7 (2) sites in China. The observed annual mean BC column concentrations in 2014 at 7 stations (Table 3) are derived from inversion based on remote sensing data and the daily variation of BC column concentration in China are evaluated by the observation at three sites in Hefei (31.8°N, 117.3°E, 36 m), Zhoushan (30.0°N, 122.2°E, 29 m) and Nanjing (32.1°N, 118.8°E, 52 m) (Zhang et al., 2020b).

2.4.2. LACs AAOD observations

We validate the model simulations using AAOD observations from 8 Aerosol Robotic Network (AERONET) sites (https://AERONET.gsfc.nasa.gov) in China (Table 4). In order to guarantee a greater number of stations and a longer observation period, the Level 1.5 dataset, which is quality-controlled and has a larger number of consecutive samples, is selected in the present study for 2014 and 2017. The AERONET AAOD is the sum of the contributions of all absorbing aerosols, i.e. dust, BrC and BC. We calculate the AAOD of LACs from AERONET based on the method of Depolarization Ratio and Single Scattering Albedo (Shin et al., 2019). The Depolarization Ratio at 1020 nm retrieved from AERONET is used to separate dust and non-dust particles according to the method of Shin et al. (2019) and the non-dust AAOD is further calculated from the non-dust SSA, which has been proved applicable to East Asia with a complex mixture of mineral dust and anthropogenic contamination (Dehkhoda et al., 2020).

2.4.3. MERRA-2 reanalysis data

The MERRA-2 is a reanalysis data based on the GEOS Model, Version 5 and Data Assimilation System, Version 5.12.4 and released in 2017 by NASA's GMAO (Gelaro et al., 2017), which is available online through the Goddard Earth Sciences Data and Information Services Center (https://disc.gsfc.nasa.gov). In the present study, we use the BC (OC) concentration and BC AAOD in the MERRA-2 data from the M2T1NXAER dataset (a time-averaged 2-dimensional monthly mean data collection), which is available since 1980, with a spatial resolution of 0.5° × 0.625° and 72 vertical layers from the surface to about 80 km.

3. Simulated BC concentrations

3.1. Evaluation of simulated BC and OC concentrations

Previous studies (Li et al., 2016; Mao et al., 2016, 2020) have shown that the GEOS-Chem model is reliable in simulating surface BC concentrations in China. This study further evaluates the performance of GEOS-Chem by using observed surface BC (OC) concentrations in China. The output height of the near-surface aerosols in GEOS-Chem is about 60 m and model results are sampled at the corresponding locations of the observation sites. As shown in Table 2, the observations of surface BC (OC) concentrations are obtained from the literatures at 7 (2) sites, which are annual, seasonal, and monthly averages for 2014 and 2017. The model simulations generally underestimate the observed BC concentrations at most sites except the Dalian site. The normalized mean bias (NMB) between the simulated and observed surface BC concentrations varies from −17.80% to 21.34% at measurement sites except Nanjing, which is generally within ±20% indicating the good performance of the GEOS-Chem model in simulating surface BC concentrations (Emery et al., 2017). Moreover, the NMB in this study is similar or even smaller than those in previous studies of GEOS-Chem simulation (Li et al., 2016; Mao et al., 2016, 2020). The discrepancies between simulated and observed BC concentrations in China are likely due to the coarse resolution of the chemical transport model and the uncertainties of emission inventories (Fu et al., 2012; Bond et al., 2013; Mao et al., 2016). In addition, the model simulations generally underestimate the observed OC concentrations based on the observations of Wang et al. (2018b), which is likely due to the failure of the model to adequately represent SOA formation (e.g., Miao et al., 2020, 2021).

In Fig. 1, we evaluate daily surface BC concentrations simulated by GEOS-Chem at Xianghe station in 2014 (Fig. 1a) and at Nanjing station in 2017 (Fig. 1b). The correlation coefficient between observed and simulated daily BC concentration is 0.40 at Xianghe in 2014 and 0.67 at Nanjing in 2017. All the correlation coefficients are statistically significant with 95% confidence from a two-tailed Student's *t*-test. Compared with the observed results, the NMB value simulated by GEOS-Chem model at Xianghe is −30.84% in 2014, and 3.57% at Nanjing in 2017. Compared with the results of previous studies (Li et al., 2016; Mao et al.,

Table 2
Observed and simulated monthly, seasonal, and annual mean surface BC (OC) concentrations (μg m^{-3}) at 7 (2) sites in China.

Aerosol	Site	Latitude (°N)	Longitude (°E)	Observation Period	BC Concentrations			Reference
					Observation	Model	NMB[a] (%)	
BC	Chongqing	29.61	106.5	2014.1–2	5.63	5.62	−0.18	(Zhong et al., 2016)
	Nanjing	32.05	118.75	2014.5.1-6.21	3.58	2.6	−27.37	(Hua et al., 2017)
	Beijing	40.04	116.41	2014	4.4	4.0	−9.09	(Ji et al., 2017)
	Shanghai	31.16	121.42	2014	3.11	2.88	−7.40	(Lan et al., 2020)
	Dalian	38.89	121.57	2014	1.64	1.99	21.34	(Xu, 2020)
	Baoji	34.35	107.16	2017.3–5	1.18	0.97	−17.80	(Zhou et al., 2021)
	Linan	30.13	119.42	2017	2.37	2.00	−15.61	(San et al., 2020)
OC	Chengdu	30.62	104.07	2014.10.23-11.18	10.4	7.24	−30.37	(Wang et al., 2018b)
	Nanjing	32.06	118.75	2017	6.04	6.12	1.09	(Li et al., 2023)

[a] Normalized mean biases between the simulated and observed surface BC (OC) concentrations.

Table 3
Observed and Simulated Annual Mean BC Column Concentrations (g m^{-2}) at 7 sites in China in 2014.

Site	Latitude(°N)	Longitude(°E)	Altitude(m)	BC column concentrations		
				Observation	Model	NMB (%)
Xian	34.23	108.93	389	0.004	0.003	−24.60
Hefei	31.79	117.31	36	0.004	0.005	14.01
Zhoushan	29.99	122.19	29	0.003	0.003	14.37
Songshan	34.52	113.00	475	0.004	0.005	27.99
Guangzhou	23.16	113.27	28	0.003	0.002	−22.67
Nanjing	32.05	118.75	52	0.004	0.005	16.13
Beijing	39.98	116.38	59	0.005	0.004	−17.72

Table 4
Observed and simulated seasonal and annual mean LACs absorption aerosol optical depth (AAOD) at 8 AERONET sites in China.

Site	Latitude(°N)	Longitude(°E)	Altitude (m)	Observation Period	LACs AAOD		
					Observation	Model	NMB(%)
Hong_Kong_PolyU	22.3	114.18	30.0	2014	0.030	0.023	−23.25
Beijing	39.98	116.38	92.0	2014	0.052	0.054	4.28
				2017	0.043	0.032	−25.97
Xianghe	39.75	116.96	36.0	2014	0.053	0.048	−9.04
				2017	0.036	0.036	−1.47
XuZhou	34.22	117.14	59.7	2017	0.043	0.052	21.80
AOE-Baotou	40.85	109.63	1314.0	2017(4–6)	0.007	0.009	19.96
Taihu	31.42	120.22	20.0	2017	0.042	0.051	22.37
Beijing_CAMS	39.93	116.32	106.0	2017	0.037	0.034	−8.91
Beijing_PKU	39.99	116.31	53.0	2017	0.043	0.033	−22.63

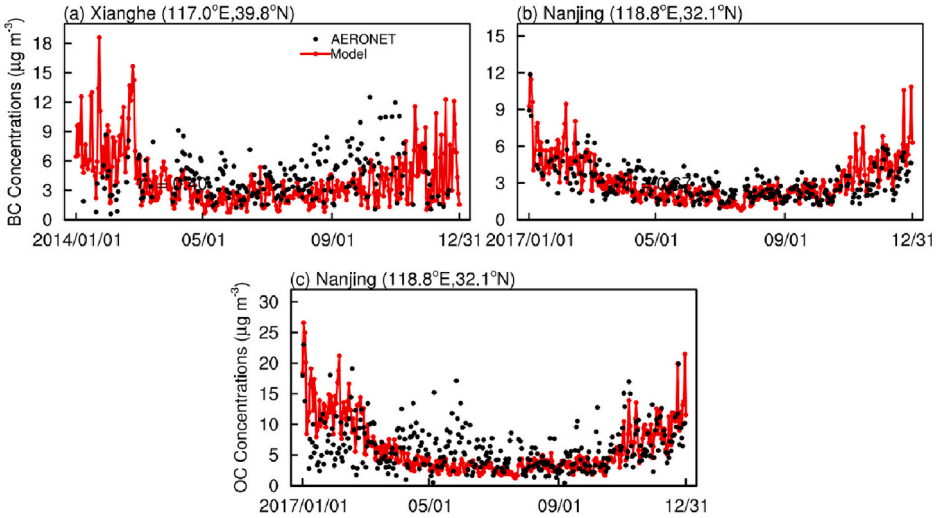

Fig. 1. Observed (black) and simulated (red) daily surface BC concentrations (μg m^{-3}) and corresponding correlation coefficient (*r*) (a) at Xianghe site in 2014 and (b) at Nanjing Caochangmen site in 2017, (c) same as (b), but for surface OC concentrations. (For interpretation of the references to colour in this figure legend, the reader is referred to the web version of this article.)

2016, 2020; Yang et al., 2017), the performance of model is acceptable, especially at Nanjing. In addition, the model fails to capture the high surface BC concentrations in October 2014 at the Xianghe site located in the North China Plain, probably because the open biomass burning emissions used in the present study underestimate heavy straw burning during corn harvest in fall (Liu et al., 2015; Yin et al., 2019). Fig. 1c also shows an assessment of the daily surface OC concentrations simulated by GEOS-Chem at Nanjing station in 2017, with the correlation coefficient of 0.44 and the NMB of −4.45% between the observed and simulated values. The model fails to capture the high OC values in Nanjing, especially in the warm seasons, which may be due to the underestimation of SOA in the model simulation (Miao et al., 2020, 2021) and open biomass burning emissions used in the study (Jin et al., 2017; Xu et al., 2019).

We evaluate the simulated annual mean BC column concentrations in 2014 by using the observations from 7 sites in Table 3. The NMB values of Xian, Songshan and Guangzhou sites are high, ranging from −24.60% to 27.99%. The remaining 4 sites (Hefei, Zhoushan, Nanjing and Beijing) show low NMB values, ranging from −17.72% to 16.13%. The simulated results are acceptable at most sites as the NMB values are all within ±30%. In Fig. 2, we evaluate the daily BC column concentrations simulated by the GEOS-Chem model at the Hefei station (Fig. 2a), Zhoushan station (Fig. 2b) and Nanjing station (Fig. 2c) in 2014. The correlation coefficients of observed and simulated daily BC column concentrations are 0.49 at Hefei, 0.53 at Zhoushan, and 0.56 at Nanjing. Compared with the observed results, the NMB value simulated by GEOS-Chem model is 14.01% at Hefei, 14.37% at Zhoushan, and 16.13% at Nanjing in 2014.

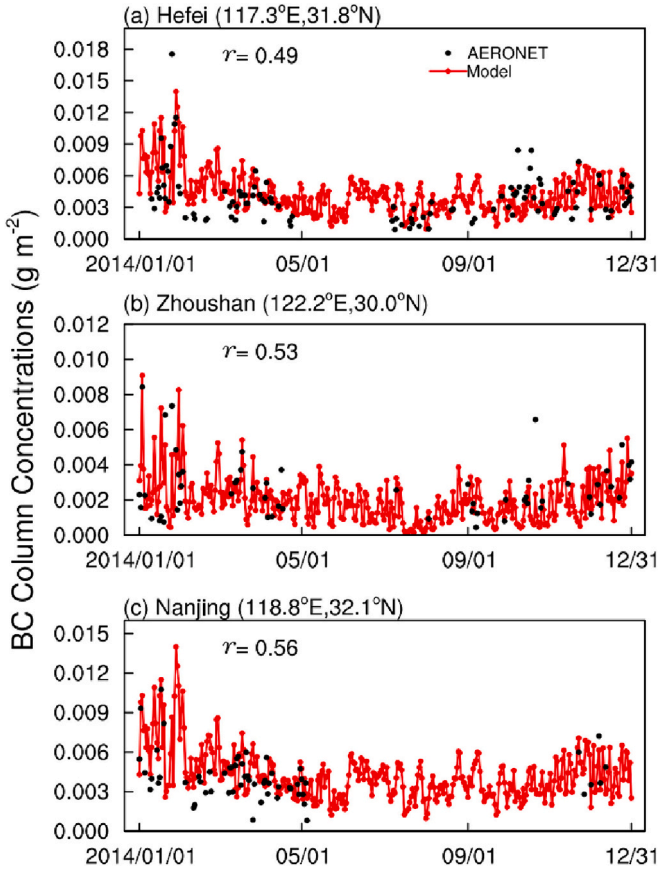

Fig. 2. Observed (black) and simulated (red) daily BC column concentrations (g m^{-2}) in 2014 and corresponding correlation coefficient (*r*) (a) at Xianghe site, (b) at Zhoushan site, (c) at Nanjing site. (For interpretation of the references to colour in this figure legend, the reader is referred to the web version of this article.)

In Fig. 3, we further use the MERRA-2 reanalysis to verify the simulation ability of GEOS-Chem on the spatial distributions of the annual mean surface BC concentration in China in 2014 and 2017. The GEOS-Chem model generally captures the characteristics of spatial distributions of surface BC concentration obtained from the MERRA-2 reanalysis data. The surface BC concentrations are high in eastern China, especially in the North China Plain. The simulated annual mean surface BC concentrations in the North China Plain range from 4 to 6 μg m^{-3} in 2014, and are lower than those from MERRA-2 reanalysis data. From 2014 to 2017, simulated surface BC concentrations decrease in eastern China, especially in the North China Plain by >1 μg m^{-3}, which are generally larger than those from the MERRA-2 reanalysis data, which is also subject to uncertainties from a low bias in historical emissions used in the assimilation system, an unrealistic representation of the boundary layer, and separating specific aerosol species based on the total aerosol optical depth included in the assimilation system (Che et al., 2024; Buchard et al., 2017).

In Fig. S1, we validate the ability of GEOS-Chem to simulate the spatial distribution of annual-averaged surface OC concentrations in China in 2014 and 2017 using MERRA-2 reanalysis. The GEOS-Chem model generally captures the characteristics of the spatial distribution of surface OC concentrations in the MERRA-2 reanalysis data. The spatial distribution of surface OC concentrations is similar to that of BC. In 2014, the simulated annual mean surface OC concentrations in the North China Plain range from 7 to 11 μg m^{-3}, which are lower than those from the MERRA-2 reanalysis data (9–15 μg m^{-3}). From 2014 to 2017, the simulated surface OC concentrations decrease by >1 μg m^{-3} (Fig. S1c) and the high values of above 2 μg m^{-3} are concentrated in the North China Plain. The MERRA-2 reanalysis data, on the other hand, shows that surface OC concentrations are reduced from 2014 to 2017, especially in the Beijing-Tianjin-Hebei and Northeast regions, with high values above 2 μg m^{-3}.

3.2. Surface BC concentrations

Fig. S2 shows the spatial distributions of seasonal and annual mean surface concentrations of BC in China simulated by the GEOS-Chem model for 2014 (Fig. S2a) and 2017 (Fig. S2b). The annual mean surface concentration of BC in China is 0.72 μg m^{-3} (0.92 μg m^{-3}) in 2017 (2014), which is low in the west and high in the east. The annual average BC concentration is highest in the North China Plain, exceeding 3.5 μg m^{-3}(4 μg m^{-3}) in 2017 (2014). Compared with the western region, the dense population and developed industry in eastern China lead to higher BC emissions. In addition, topographic factors can also affect the distribution of BC, which induce high BC concentrations in the areas, e.g., Sichuan Basin and western part of North China Plain (Liu et al., 2018b).

The seasonal mean BC concentration in China is highest in December–January-February (DJF), about 1.19 μg m^{-3} (1.48 μg m^{-3}) in 2017 (2014). In DJF, high concentrations of BC locate in the North China Plain and central China, with the values >5 μg m^{-3} (6 μg m^{-3}) in 2017 (2014). The Northeast Plain also has a high BC concentration in DJF, with the value exceeding 3 μg m^{-3}. The high concentration of BC in DJF is likely due to the enhanced anthropogenic emission by the combustion of heating fuel, as well as the lower temperature, weaker wind speed, and less precipitation, which are not conducive to the diffusion and removal of pollutant (Fu et al., 2012). In June–July-August (JJA), the seasonal

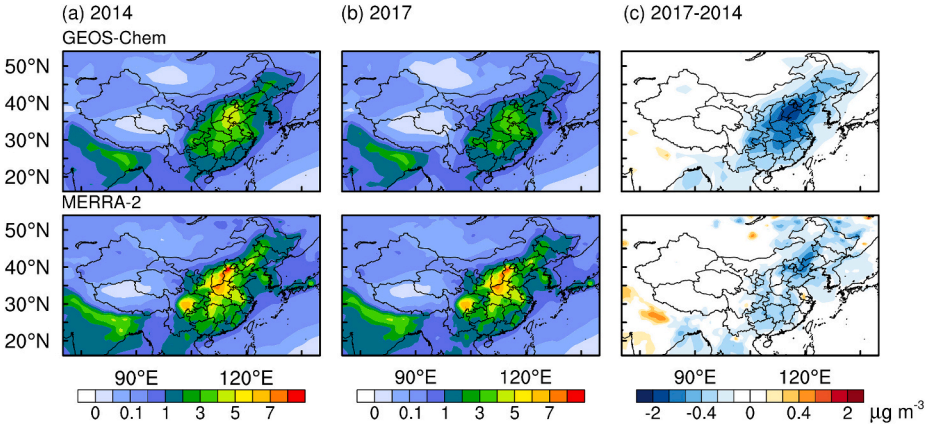

Fig. 3. (a) Annual mean surface BC concentrations (μg m^{-3}) in China in 2014, (b) same as (a), but in 2017, (c) differences of annual mean surface BC concentrations in China between 2017 and 2014. Firstrow from the GEOS-Chem simulation, second row from the MERRA-2 reanalysis data.

mean concentration of BC in China is lowest, about 0.47 μg m^{-3} (0.59 μg m^{-3}) in 2017 (2014) and the high concentrations of BC are distributed in central China and the Yangtze River Delta (around 3 μg m^{-3} in 2014 and around 2 μg m^{-3} in 2017). The reduced heating fuel burning, the prevalence of summer monsoon and thus increased wet deposition all contribute to low BC concentrations in JJA (Fu et al., 2012).

Fig. S2c shows the changes of simulated seasonal and annual mean surface BC concentrations in China from 2014 and 2017. From 2014 to 2017, the annual average surface BC concentration in China decreases by 0.20 μg m^{-3}, largely due to the significantly decrease of BC anthropogenic emissions in China by ~23% from 2014 to 2017 after the release of the APPCAP (Zheng et al., 2018). The reduction of the annual mean BC concentration is largest in densely populated areas in eastern China, reaching 1.54 μg m^{-3}. In March–April-May (MAM), September–October-November (SON) and DJF, the spatial distribution of the changes of surface BC concentration between the two years is generally consistent with that of annual average surface BC concentration. The decrease of seasonal mean BC concentration is the largest in DJF, with a mean value of 0.29 μg m^{-3} and a maximum value of 3.01 μg m^{-3} in the North China Plain.

4. Simulated LACs AAOD

4.1. Evaluation of simulated LACs AAOD

Table 4 compares AERONET derived and GEOS-Chem simulated annual mean LACs AAOD at 8 AERONET sites in China. The NMB values between the simulated and observed LACs AAOD are lower in 2014 than in 2017. Compared with the observations in 2014, the NMB value of the simulated LACs AAOD at Hong_Kong_PolyU site is −23.25%, and those at the other sites vary from −9.04% to 4.28%. In 2017, the NMB values of simulated LACs AAOD are large at the Beijing, Xuzhou, Taihu and Beijing_PKU sites, ranging from −25.97% to 22.37%, and are low at the other three sites. In particular, the NMB values of LACs AAOD at the Xianghe and Beijing-CAMS sites range from −8.91% to −1.47% in 2017. Compared with previous studies (Li et al., 2016; Mao et al., 2016), the NMB value between the simulated and the observed AAOD is smaller, likely due to removing dust in the calculation of LACs AAOD at the AERONET sites, updating the complex refractive index of BC, and adding the absorbent BrC in the present GEOS-Chem simulation.

In Fig. 4, we further evaluate the daily variation of LACs AAOD at 440 nm simulated by GEOS-Chem model at 3 AERONET sites in Beijing and Xianghe in 2014 and 2017. The AERONET derived LACs AAOD generally shows high values around 0.20 in DJF and second-high values above 0.10 in March, October and November. Overall, the model is able to capture the seasonal characteristics of the LACs AAOD in 2014 and 2017. In 2017 (2014), the correlation coefficients of observed and simulated daily LACs AAOD are 0.82 (0.64) at Beijing, 0.68 (0.63) at Xianghe, 0.78 at Beijing-CAMS and 0.76 at Beijing-PKU. The NMB values of observed and simulated LACs AAOD in 2017 (2014) are −25.97% (4.28%) at Beijing, −1.47% (−9.04%) at Xianghe, −8.91% at Beijing-CAMS, and − 22.63% at Beijing-PKU.

We further use MERRA-2 reanalysis data to compare and validate simulated BC AAOD. Fig. S3 shows the spatial distributions of BC annual average AAOD at 550 nm in China from the GEOS-Chem model and the MERRA-2 reanalysis data in 2014 and 2017. The spatial distributions and the values of annual average BC AAOD from the GEOS-Chem simulation are in good agreement with those from the MERRA-2 reanalysis data. Similar to the BC surface concentrations, the areas with high values of BC AAOD are mainly distributed in the North China Plain and

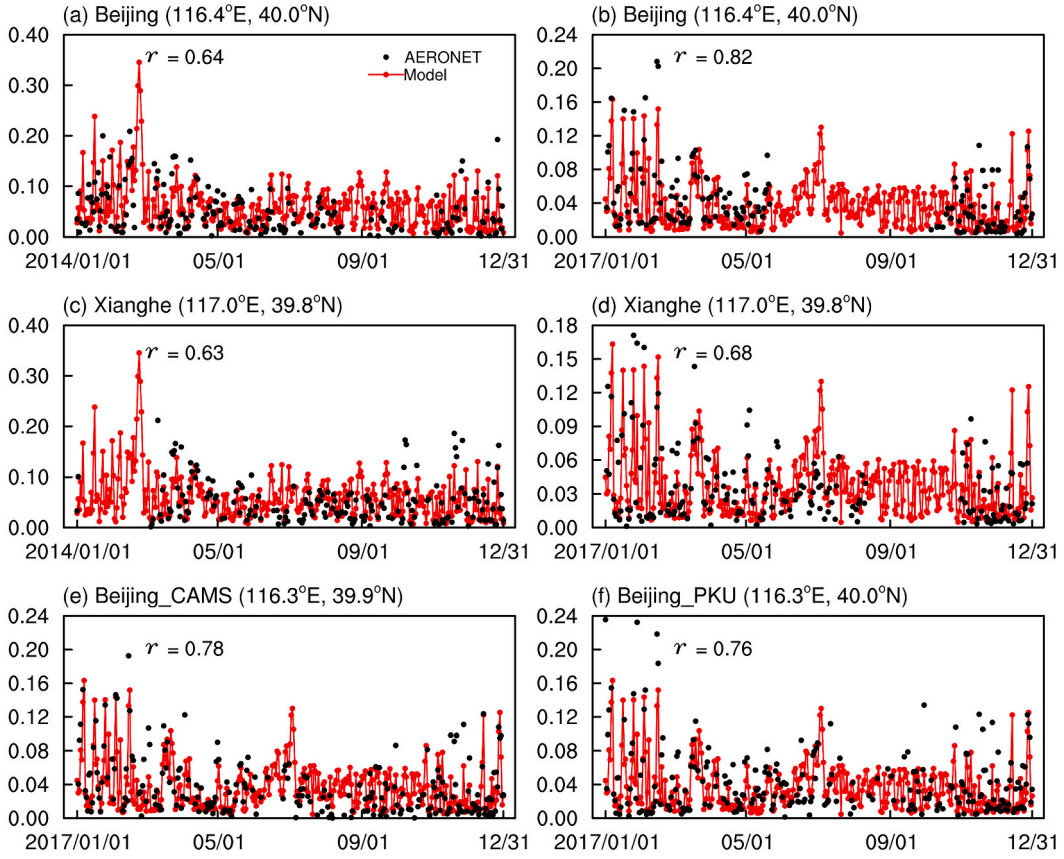

Fig. 4. AERONET observed (black) and GEOS-Chem simulated (red) daily LACs absorption aerosol optical depth (AAOD) at 440 nm and corresponding correlation coefficient (*r*). (a) at Beijing site in 2014, (b) at Beijing site in 2017, (c) at Xianghe site in 2014, (d) at Xianghe site in 2017, (e) at Beijing_CAMS site in 2017, (f) at Beijing_PKU site in 2017. (For interpretation of the references to colour in this figure legend, the reader is referred to the web version of this article.)

Sichuan Basin. The high values from the GEOS-Chem simulation are 0.040–0.060 in 2014 and 0.030–0.040 in 2017, and those from the MERRA-2 reanalysis data range from 0.040 to 0.050. The GEOS-Chem simulated BC AAOD decreases from 2014 to 2017, and the changes are significantly in eastern China and Sichuan Basin (> 0.010). The changes are larger from the GEOS-Chem simulation than from the MERRA-2 reanalysis data, which may be partially due to the updated BC refractive index used in the GEOS-Chem simulation.

4.2. BC AAOD

Fig. S4 shows the spatial distribution of seasonal and annual mean BC AAOD at 440 nm in China simulated by the GEOS-Chem model in 2014 (Fig. S4a) and 2017 (Fig. S4b). The annual mean BC AAOD is 0.013 (0.017) in 2017 (2014) in China, and the spatial distribution of annual mean BC AAOD in China in the two years is similar to that of BC concentration, with low values in the west and high values in the east. The annual mean BC AAOD is high in the North China Plain and Sichuan Basin ranging from 0.040 to 0.060 (0.060 to 0.080) in 2017 (2014), with the highest value of 0.058 (0.073) in 2017 (2014) in the Sichuan Basin.

Similar to the BC concentration, the seasonal mean BC AAOD is highest in DJF by 0.017 (0.022) in 2017 (2014). The high values of BC AAOD in DJF are in the Sichuan Basin and the eastern part of the North China Plain, exceeding 0.070 (0.080) in 2017 (2014), which are close to results from the study of Li et al. (2016). In DJF, the simulated BC AAOD in Sichuan is higher at lower BC concentrations compared with that in Beijing-Tianjin-Hebei. In JJA, BC AAOD can reach high levels at relatively low BC concentrations likely due to strong solar radiation and high humidity (He et al., 2015, Tang et al., 2021). The high value of BC AAOD in JJA is in the North China Plain by about 0.040 (0.050) in 2017 (2014).

Fig. S4c shows the changes of simulated seasonal and annual mean BC AAOD in China from 2014 to 2017. Due to the significant reduction of BC emissions during the implementation of APPCAP, the annual average BC AAOD in China decreases by 0.004 from 2014 to 2017, with the contribution from anthropogenic sources by 89%. In DJF, the seasonal mean BC AAOD decreases by 0.004, and the largest reduction of BC AAOD is 0.030 in the southern region of Beijing-Tianjin-Hebei. The decline of the seasonal mean BC AAOD in JJA is about 0.003, mainly concentrated in central China.

4.3. BrC AAOD

Fig. 5 shows the spatial distribution of the seasonal and annual mean BrC AAOD at 440 nm in China simulated by GEOS-Chem in 2014 (Fig. 5a) and in 2017 (Fig. 5b). The annual mean values of BrC AAOD in

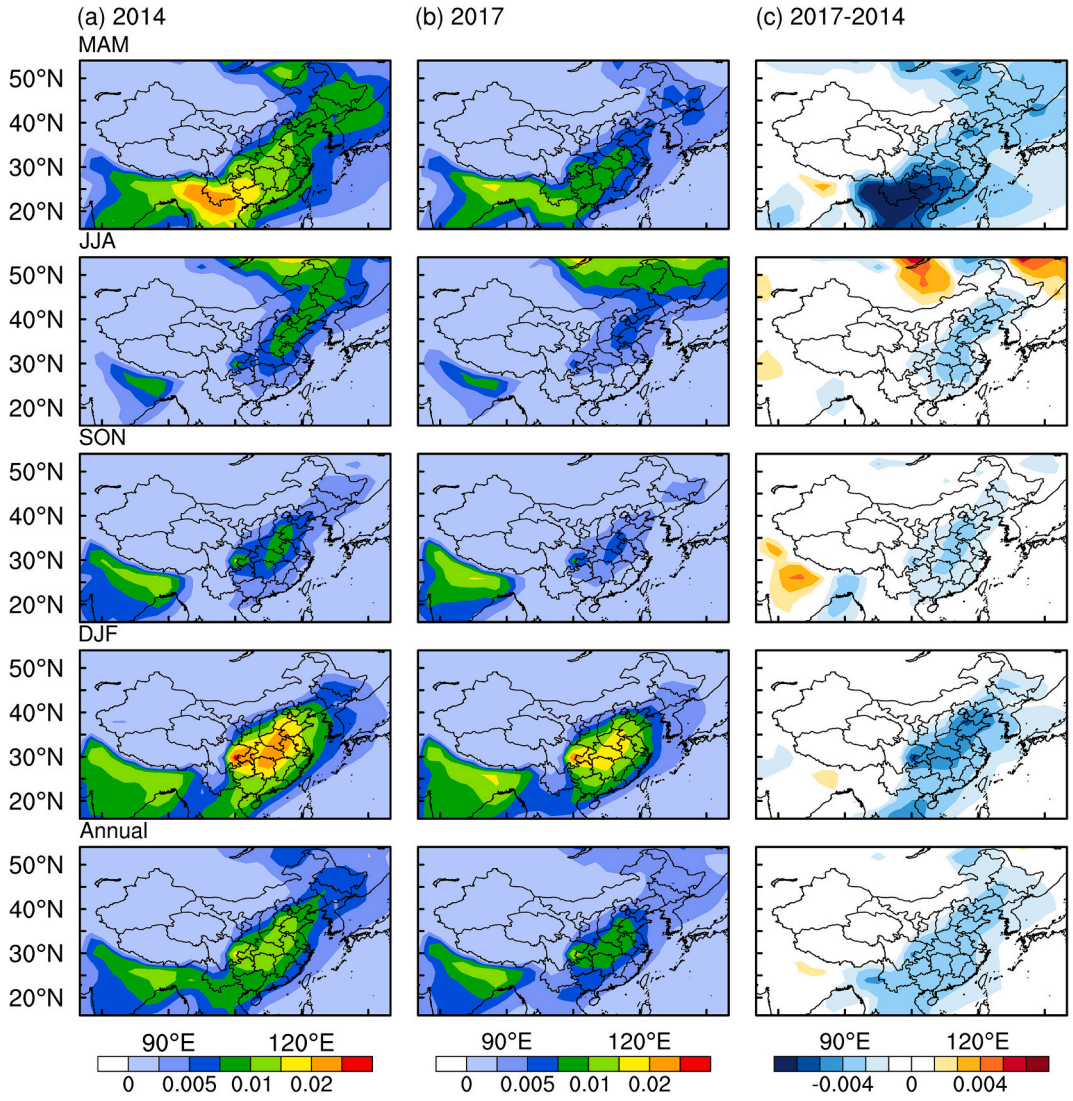

Fig. 5. (a) Simulated seasonal and annual average BrC AAOD at 440 nm in China in 2014, (b) same as (a), but in 2017, (c) differences in simulated seasonal and annual average BrC AAOD in China between 2017 and 2014.

China are 0.003 in 2017 and 0.004 in 2014, with the BF sources contributing up to 50% and 48%, followed by the BB (31% and 36%) and CC (19% and 16%) sources. Similar to BC AAOD, the annual mean BrC AAOD in China also shows high values in the eastern area and low values in the western area. And the annual mean BrC AAOD is highest in Sichuan Basin, with the values of approximately 0.010 in 2017 and 0.015 in 2014.

The seasonal mean BrC AAOD in China is highest in MAM by 0.004 in 2017 and 0.006 in 2014, with the largest contribution from the BB sources by 43% in 2017 and 57% in 2014. In MAM, the high BrC AAOD is mainly distributed in southwestern China with values ranging from 0.015 to 0.020 in 2014 and around 0.010 in 2017, likely due to the local fires in the Yunnan-Guizhou Plateau and southeastern hills (Wang et al., 2022b) and long-distance transport of pollutants from forest fires and agricultural biomass burning in the countries of Indochina from November to March (Deng et al., 2008; Fan et al., 2023; Fu et al., 2011; Lian et al., 2022; Zhu et al., 2017). In addition, in MAM, BrC AAOD is also high in northeast China, which may be attributed to forest fires in and around Northeast China (Fan et al., 2017; Zhu et al., 2023) and open burning of straw before spring ploughing in northeastern plains (Ma et al., 2018). In JJA, the seasonal mean BrC AAOD in China is relatively close in 2017 and 2014 (around 0.003) and is high in northeastern China bordering Inner Mongolia and extending southward to the North China Plain, with the largest contribution (60% in 2017 and 56% in 2014) from smoke plumes of forest fires in the Russian Far East and Siberia during the summer (Zhu et al., 2018). In DJF, the seasonal average BrC AAOD value is 0.004 (0.005) in 2017 (2014), with the largest contributions from the BF and CC sources (68% and 25% in 2017, 70% and 23% in 2014). High values of BrC AAOD in DJF are found in central China with values above 0.015 (0.020) in 2017 (2014). In SON, the seasonal mean BrC AAOD value in China is the smallest, all around 0.002 in 2017 and 2014.

Fig. 5c shows the decrease in modeled seasonal and annual mean BrC AAOD in China from 2014 to 2017. From 2014 to 2017, the annual mean BrC AAOD decreases by 0.001 in China. The BB source is the largest contributor (48%) to the reduction of the annual mean BrC AAOD, followed by BF (43%) and CC (9%). In MAM, the seasonal mean BrC AAOD decreases by 0.0025 from 2014 to 2017, and BrC AAOD from BB sources decreases by 0.002 (77%). The largest decrease of BrC AAOD locates in southwestern China with the largest values of 0.020, mainly due to the decrease in emissions from forests and shrubland fires in southwestern China and neighboring countries (Reddy et al., 2020; Huang et al., 2021). The seasonal mean BrC AAOD in MAM also decreases in Northeast China Plain, with the main contributing from BB source (70%), which is attributed to the decreased forest fires (Zhu et al., 2023) and straw-burning ban policy implemented in Northeast China during spring ploughing (Fu et al., 2022; Yang et al., 2020). In DJF, the seasonal mean BrC AAOD decreases by 0.001, largely due to the contribution of the BF source by 77%, followed by the CC (14%) and BB (8%) sources. The largest reduction of BrC AAOD is mainly distributed in Sichuan Basin

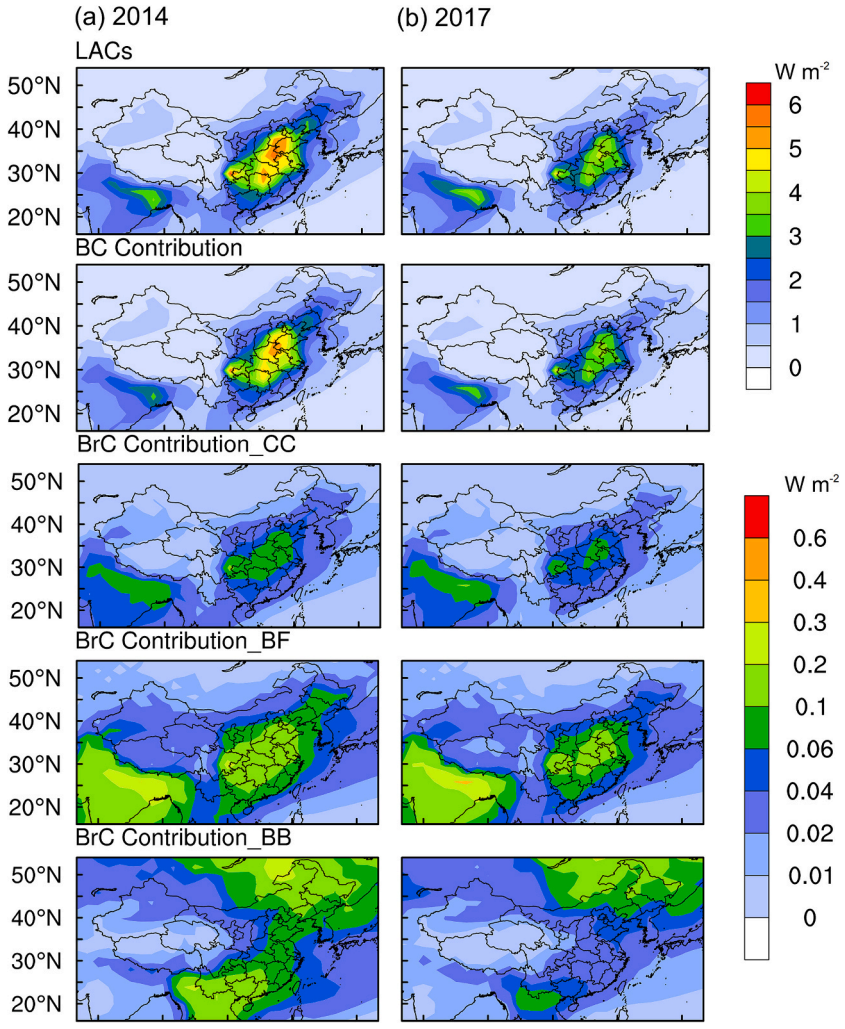

Fig. 6. (a) Simulated annual mean clear-sky direct radiative forcing (DRF) of LACs, BC and BrC (W m^{-2}) at the top of the atmosphere (TOA) from biomass burning source, and coal combustion and biofuel combustion in residential sector in China in 2014, (b) same as (a) but in 2017.

with the values ranging from 0.006 to 0.010, which is mainly due to the reduction of emissions from fuel combustion sources in the residential sector as a result of the implementation of the clean energy policy and the coal ban (Ji et al., 2022; Meng et al., 2019; Zheng et al., 2018).

5. Simulated Direct Radiative Forcing of LACs

Fig. 6 shows the spatial distribution of annual mean clear-sky LACs DRF at TOA in China in 2014 and 2017 simulated by the coupled GEOS-Chem-RRTMG model, and the contributions from BC and BrC. In China, the annual mean value of the LACs DRF is 1.02 W m^{-2} (1.38 W m^{-2}) in 2017 (2014). The high values of annual mean LACs DRF are mainly located in the North China Plain, the central China, and the Sichuan Basin, ranging from 4 to 6 W m^{-2} in 2014 to 3–5 W m^{-2} in 2017. The distribution of the high value of annual mean LACs DRF is similar to that of BC DRF, as BC is the largest contributor to LACs DRF, reaching 90% (89%) in 2017 (2014).

5.1. BC DRF

Fig. 7 shows the spatial distributions of seasonal and annual mean clear-sky DRF of BC at TOA in China simulated by the GEOS-Chem model for 2014 (Fig. 7a) and 2017 (Fig. 7b). The annual mean value of BC DRF in China is 0.91 W m^{-2} (1.23 W m^{-2}) in 2017 (2014), and is smaller compared with those from the previous studies (1.22 W m^{-2} to 3.0 W m^{-2}, Li et al., 2016; Liu et al., 2022; Yang et al., 2017), which is likely related to the decline in simulated BC concentrations due to the implementation of emission reduction policies and the differences in the setting of the BC optical properties (Liu et al., 2022; Yang et al., 2017).

Similar to the distribution of BC concentration and AAOD, the seasonal mean value of BC DRF is highest in DJF, which is 1.14 W m^{-2} (1.42 W m^{-2}) in China in 2017 (2014) and the high values of BC DRF are located in the Sichuan Basin and central-eastern China, ranging from 5.50 to 8.50 W m^{-2} (6.00 to 7.50 W m^{-2}). In JJA, the seasonal mean value of BC DRF in China is 0.82 W m^{-2} (1.15 W m^{-2}) in 2017 (2014), higher than that in SON by 0.65 W m^{-2} (0.89 W m^{-2}). The high values of BC DRF in JJA are located in the North China Plain, with 3.50–5.00 W m^{-2} (4.50–6.50 W m^{-2}) in 2017 (2014).

Fig. 7c shows the changes in simulated seasonal and annual mean BC DRF in China between 2017 and 2014. From 2014 to 2017, the annual average BC DRF in China decreases by 0.32 W m^{-2}, which is largely attributed to the anthropogenic sources by 88%. In terms of seasonal changes, the BC DRF decreases largest in JJA, mainly concentrated in the central China by above 1.60 W m^{-2}. In DJF (SON), the large decrease of BC DRF is mainly concentrated on northern China, by up to 1.88 W m^{-2} (1.67 W m^{-2}), which is related to the reduction of BC emissions due to the promotion of clean energy heating in winter and the straw burning ban in the autumn harvest season (Meng et al., 2019).

5.2. BrC DRF

Fig. 8 shows the spatial distribution of seasonal and annual mean clear sky BrC DRF at TOA in China in 2014 (Fig. 8a) and 2017 (Fig. 8b) simulated by the GEOS-Chem-RRTMG model. The annual mean of BrC DRF in China is 0.11 W m^{-2} in 2017 and 0.15 W m^{-2} in 2014, dominated by the BF source (46% in 2017 and 44% in 2014) and the BB source (38% in 2017 and 43% in 2014), with CC source being low (16% in 2017 and 13% in 2014). Compared to the values (0.04–0.11 W m^{-2}) reported

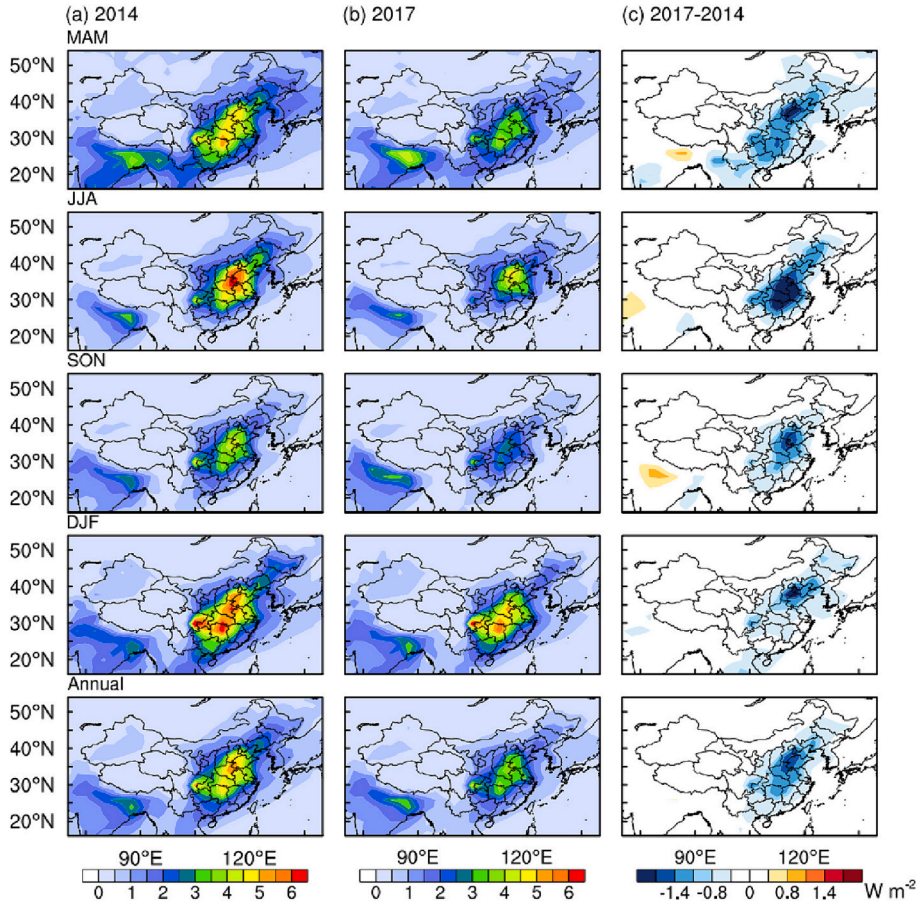

Fig. 7. (a) Simulated seasonal and annual average clear-sky TOA DRF of BC in China in 2014, (b) same as (a), but in 2017, (c) differences in simulated seasonal and annual average clear-sky TOA DRF of BC in China between 2017 and 2014.

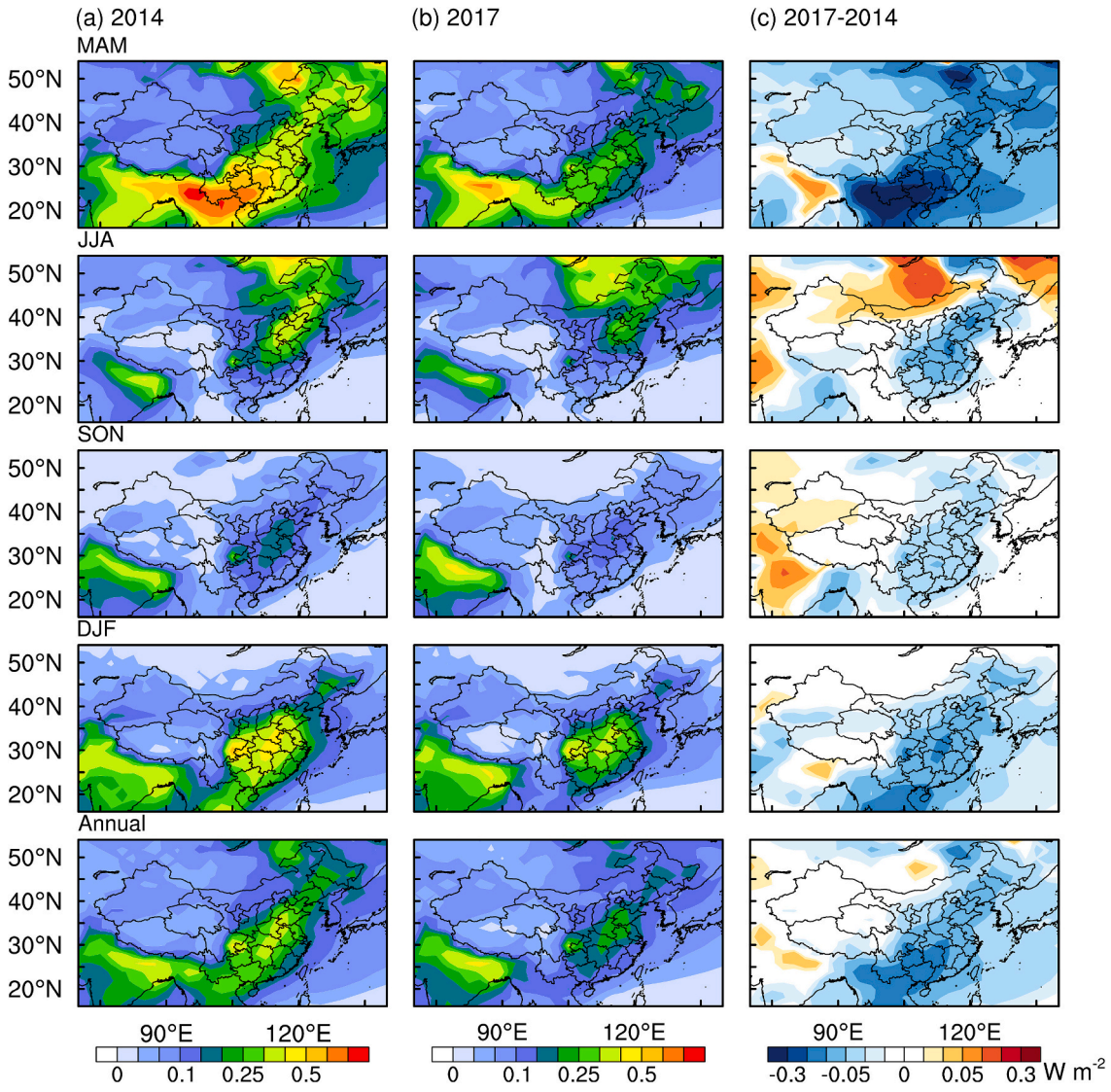

Fig. 8. (a) Simulated seasonal and annual average clear-sky TOA DRF of BrC in China in 2014, (b) same as (a), but in 2017, (c) differences in simulated seasonal and annual average clear-sky TOA DRF of BrC in China between 2017 and 2014.

in previous studies (Brown et al., 2018; Feng et al., 2013; Jo et al., 2016; Wang et al., 2014, 2018a; Zhang et al., 2021a), the BrC DRF estimated in the present study is at a high level, which may be due to the differences in the emission and optical properties of BrC used in the model. The BrC DRF in southwestern and northeastern China (Fig. 6) shows large contribution to the LACs DRF by about 10–30%, which is related to local biomass combustion (Fan et al., 2017; Lian et al., 2022; Ma et al., 2018; Tian et al., 2013) and the transmission of biomass combustion in neighboring areas (Duc et al., 2016; Zhu et al., 2017, 2018).

Similar to the BrC AAOD, the seasonal mean BrC DRF in China is highest in MAM, by 0.15 W m^{-2} (0.25 W m^{-2}) in 2017 (2014), with the largest contribution from the BB source by 45% (60%) in 2017 (2014). In MAM, southwestern China and northeast China are the main regions with high values of BrC DRF, by >0.60 W m^{-2}, which is related to the large amount of open air biomass burning in the local and surrounding region (Ma et al., 2018; Zhu et al., 2017, 2018). In JJA, the seasonal mean BrC DRF in China is 0.11 W m^{-2} (0.13 W m^{-2}) in 2017 (2014), with the largest contribution from BB sources by 62% (57%) in 2017 (2014). In JJA, the northeastern China plain has a high value of BrC DRF due to the transport of carbonaceous aerosols from forest fire in Russia and Mongolia (Zhu et al., 2018). In DJF, the seasonal mean BrC DRF value is 0.11 W m^{-2} (0.14 W m^{-2}) in 2017 (2014) with the largest contribution from the BF and CC sources by 67% and 22% (69% and 21%), respectively, and the highest seasonal mean BrC DRF values are mainly distributed in the North China Plain, Sichuan Basin, and Central China. In SON, the seasonal mean BrC DRF value is the smallest , about 0.06 W m^{-2} (0.07 W m^{-2}) in 2017 (2014) in China.

Fig. 8c shows the reduction of simulated seasonal and annual mean BrC DRF in China between 2017 and 2014. In 2017, the annual mean BrC DRF in China decreases by 0.04 W m^{-2} from 2014, significantly in southwestern China by >0.10 W m^{-2}. Due to a decrease in BB emissions (Fig. S5), the BB source is the largest contributor to the reduction of annual mean BrC DRF (by 56%), followed by BF (36%) and CC (8%). Similar to BrC AAOD, the seasonal mean BrC DRF declines most dramatically in MAM by 0.11 W m^{-2} from 2014 to 2017, with the largest contribution from the BB source (81%), and the reduction is mainly distributed in southwestern China by up to 0.30 W m^{-2}, likely attributed to the reduced emissions from natural sources, such as forests and shrubland fires in the local and neighboring areas (Reddy et al., 2020; Huang et al., 2021). Similar to BrC AAOD, the seasonal mean BrC DRF also declines in Northeast China Plains in MAM, with regional means values up to about 0.12 W m^{-2}, and the main contribution is from the BB source (76%), which is attributed to the reduction of emissions from agricultural and forest fire sources in the local and neighboring areas (Fu

et al., 2022; Yang et al., 2020; Zhu et al., 2023). In DJF, the seasonal mean BrC DRF decreases by about 0.03 W m^{-2}, which is mainly due to the contribution of the BF source (75%), followed by the CC source (17%) and the BB source (8%). The high value of the BrC DRF decline is located in the central-eastern part of China and can reach up to 0.10 W m^{-2}. In JJA, BrC DRF decreases by 0.02 W m^{-2}, mainly due to reduced BF source (69%), followed by BB (17%) and CC (14%). The decreased BrC DRF could be as high as 0.10 W m^{-2} in JJA, mainly distributed in central and northern China, which may be related to the reduction of carbonaceous aerosol emissions during the summer harvest season after the implementation of straw burning ban policy (Tang et al., 2020b).

6. Discussions

There are large uncertainties in the estimates of LACs DRF in the present study. The BC particles are simply assumed to be spherical and external mixed in the GEOS-Chem model. Studies have shown that the complex particle structures/morphology would significantly affect the optical properties and hence radiative properties of BC. For example, Luo et al. (2022) showed that compared to fractal structures, spherical structures can lead to a reduction of the BC AAOD by 8% and the regionally averaged BC aerosol-radiation interaction by 17.1–38.7%. The absorption cross-section of internally mixed coated BC may increase by 20–250% compared to externally mixed, depending on the coating structure and morphology (He et al., 2015). The researches using microphysics schemes (e.g., He et al., 2016; Chen et al., 2017) show that there are great differences in the aging time of BC in China, and a fixed e-folding time of 1.15 days used to parameterize BC aging in the present study would also bring errors to the simulations of BC concentration and its optical properties. Meanwhile, the absorption enhancement factor (E_{abs}) of BC generally varies widely in the range of 1–3.5 (Cappa et al., 2012; Chung et al., 2012; Cui et al., 2016; Peng et al., 2016; Zhang et al., 2008), as obtained from many observations and studies based on optical model. The fundamental reason for the difference in E_{abs} of BC is in the degree of aging, and the E_{abs} of BC changes dynamically in different regions, periods, and pollution conditions (Li et al., 2024; Tan et al., 2020). The use of a fixed single E_{abs} of 1.5 recommended by Bond et al. (2006) thus likely introduce large errors in the estimation of the AAOD and DRF. As for BrC, we use an assumed BC/OC emission ratio to distinguish between CC and BF, and observed BC/OC and MAE to parameterize the optical properties of BB/BF and CC, respectively, all of which would introduce uncertainty into the modeling results. Finally, secondary BrC was not considered in the present study. Although many studies have shown that SOA has significantly lower light absorption than POA (Martinsson et al., 2015; Ni et al., 2021; Saleh et al., 2013; Wang et al., 2016), ignoring SOA would also result in an underestimation of the DRF of LACs (Wang et al., 2019).

7. Conclusions

We used the coupled GEOS-Chem-RRTMG model to investigate temporal and spatial variations of the AAOD and DRF of LACs over China during the implementation of APPCAP. We updated the refractive index of BC and included solid fuel combustion in the residential sector and open-air biomass burning as sources of BrC, and distinguish the optical properties of BrC from different combustion sources.

Our results showed that model could reasonably capture the spatial and temporal variations of LACs in China. Compared to the daily observations from 4 AERONET sites in Beijing and Xianghe, the observed and simulated biases of the LACs AAOD at 440 nm were from −25.97% to −1.47% (−9.04%–4.28%) in 2017 (2014) and the corresponding correlation coefficients were >0.63. The simulated annual mean LACs AAOD at 440 nm in China was 0.016 (0.021) in 2017 (2014), with the contributions of 80% (79%) from BC and 20% (21%) from BrC. The contribution of the BF source to BrC AAOD was the highest by 50% in 2017 and 48% in 2014, followed by the BF (31% and 36%) and CC sources (19% and 16%).

The simulated annual mean clear-sky LACs DRF at TOA in China was 1.02 W m^{-2} (1.38 W m^{-2}) in 2017 (2014), with the contribution of 90% (89%) from BC and 10% (11%) from BrC. The simulated annual mean BC DRF in China was 0.91 W m^{-2} in 2017 (1.23 W m^{-2} in 2014). From 2014 to 2017, BC DRF in China decreased significantly, with the contribution from anthropogenic sources by 88%, largely related to the implementation of APPCAP. The simulated annual mean BrC DRF was dominated by the BF source (46% in 2017 and 44% in 2014), followed by the BB (38% in 2017 and 43% in 2014) and CC (16% in 2017 and 13% in 2014) sources, and the high values were mainly located in the eastern China by >0.2 W m^{-2} in 2017 and 0.3 W m^{-2} in 2014. The present study would improve the understanding of the climate effects of LACs in China during the implementation of APPCAP.

Author contributions statement

Liu Yang: Investigation, Data curation, Visualization, Writing-Original draft preparation; Yuhao Mao: Conceptualization, Methodology, Writing-Reviewing and Editing; Hong Liao: Conceptualization; Mingjie Xie: Data curation; Ying Zhang: Data curation.

CRediT authorship contribution statement

Liu Yang: Investigation, Data curation, Visualization, Writing – original draft. **Yuhao Mao:** Conceptualization, Methodology, Writing – review & editing. **Hong Liao:** Conceptualization. **Mingjie Xie:** Data curation. **Ying Zhang:** Data curation.

Declaration of competing interest

The authors declare no conflicts of interest.

Data availability

Data will be made available on request.

Acknowledgment

This work was supported by the Innovative Research Group Project of National Natural Science Foundation of China (grant no. 42021004) and Natural Science Foundation of Jiangsu Province (grant no. BK20220031). We acknowledge the High-Performance Computing Centre of Nanjing University of Information Science and Technology for their support of this work.

Supplementary data

Supplementary data to this article can be found online at https://doi.org/10.1016/j.atmosres.2024.107396.

References

Akagi, S.K., Yokelson, R.J., Wiedinmyer, C., Alvarado, M.J., Reid, J.S., Karl, T., Crounse, J.D., Wennberg, P.O., 2011. Emission factors for open and domestic biomass burning for use in atmospheric models. Atmos. Chem. Phys. 11, 4039–4072.
Andreae, M.O., Gelencser, A., 2006. Black carbon or brown carbon? The nature of light-absorbing carbonaceous aerosols. Atmos. Chem. Phys. 6, 3131–3148.
Bhat, M.A., Romshoo, S.A., Beig, G., 2017. Aerosol black carbon at an urban site-Srinagar, Northwestern Himalaya, India: Seasonality, sources, meteorology and radiative forcing. Atmos. Environ. 165, 336–348.
Bond, T.C., Bergstrom, R.W., 2006. Light Absorption by Carbonaceous Particles: an Investigative Review. Aerosol Sci. Technol. 40 (1), 27–67.
Bond, T.C., Habib, G., Bergstrom, R.W., 2006. Limitations in the enhancement of visible light absorption due to mixing state. J. Geophys. Res. Atmos. 111 (D20), D20211.
Bond, T.C., Bhardwaj, E., Dong, R., Jogani, R., Jung, S., Roden, C., Streets, D.G., Trautmann, N.M., 2007. Historical emissions of black and organic carbon aerosol from energy-related combustion, 1850–2000. Glob. Biogeochem. Cycles 21 (2), 2006GB002840.

Bond, T.C., Doherty, S.J., Fahey, D.W., Forster, P.M., Berntsen, T., DeAngelo, B.J., Flanner, M.G., Ghan, S., Kärcher, B., Koch, D., Kinne, S., Kondo, Y., Quinn, P.K., Sarofim, M.C., Schultz, M.G., Schulz, M., Venkataraman, C., Zhang, H., Zhang, S., Bellouin, N., Guttikunda, S.K., Hopke, P.K., Jacobson, M.Z., Kaiser, J.W., Klimont, Z., Lohmann, U., Schwarz, J.P., Shindell, D., Storelvmo, T., Warren, S.G., Zender, C.S., 2013. Bounding THE role of black carbon in THE climate system: a scientific assessment: BLACK CARBON IN THE CLIMATE SYSTEM. J. Geophys. Res. Atmos. 118 (11), 5380–5552.

Brown, H., Liu, X., Feng, Y., Jiang, Y., Wu, M., Lu, Z., Wu, C., Murphy, S., Pokhrel, R., 2018. Radiative effect and climate impacts of brown carbon with the Community Atmosphere Model (CAM5). Atmos. Chem. Phys. 18 (24), 17745–17768.

Buchard, V., Randles, C.A., Da Silva, A.M., Darmenov, A., Colarco, P.R., Govindaraju, R., Ferrare, R., Hair, J., Beyersdorf, A.J., Ziemba, L.D., Yu, H., 2017. The MERRA-2 Aerosol Reanalysis, 1980 Onward. Part II: Evaluation and Case Studies. J. Clim. 30 (17), 6851–6872.

Cappa, C.D., Onasch, T.B., Massoli, P., Worsnop, D.R., Bates, T.S., Cross, E.S., Davidovits, P., Hakala, J., Hayden, K.L., Jobson, B.T., Kolesar, K.R., Lack, D.A., Lerner, B.M., Li, S.-M., Mellon, D., Nuaaman, I., Olfert, J.S., Petäjä, T., Quinn, P.K., Song, C., Subramanian, R., Williams, E.J., Zaveri, R.A., 2012. Radiative Absorption Enhancements due to the Mixing State of Atmospheric Black Carbon. Science. 337 (6098), 1078–1081.

Che, H.Z., Xia, X.A., Zhao, H.J., Li, L., Gui, K., Zheng, Y., Song, J.J, Qi, B., Zhu, J., Miao, Y.C., Wang, Y.Q., Wang, Z.L., Wang, H., Dubovik, O., Holben, B., Chen, H.B., Shi, G.Y., Zhang, X.Y., 2024. Aerosol optical and radiative properties and their environmental effects in China: A review. Earth-Science Reviews 248, 104634.

Chen, Y., Bond, T.C., 2010. Light absorption by organic carbon from wood combustion. Atmos. Chem. Phys. 10 (4), 1773–1787.

Chen, X.S., Wang, Z.F., Yu, F., Pan, X.L., Li, J., Ge, B., Wang, Z., Hu, M., Yang, W.Y., Chen, H.S., 2017. Estimation of atmospheric aging time of black carbon particles in the polluted atmosphere over Central-Eastern China using microphysical process analysis in regional chemical transport model. Atmos. Environ. 163, 44–56.

Cheng, Y.F., He, K.B., Zheng, M., Duan, F.K., Du, Z.Y., Ma, Y.L., Tan, J.H., Yang, F.M., Liu, J.M., Zhang, X.L., Weber, R.J., Bergin, M.H., Russell, A.G., 2011. Mass absorption efficiency of elemental carbon and water-soluble organic carbon in Beijing, China. Atmos. Chem. Phys. 11 (22), 11497–11510.

Cheng, Y., He, K.B., Du, Z.Y., Engling, G., Liu, J.M., Ma, Y.L., Zheng, M., Weber, R.J., 2016. The characteristics of brown carbon aerosol during winter in Beijing. Atmos. Environ. 127, 355–364.

Cheng, Y., He, K.B., Engling, G., Weber, R., Liu, J., Du, Z.Y., Dong, S.P., 2017. Brown and black carbon in Beijing aerosol: Implications for the effects of brown coating on light absorption by black carbon. Sci. Total Environ. 599, 1047–1055.

Chung, C.E., Lee, K., Müller, D., 2012. Effect of internal mixture on black carbon radiative forcing. Tellus Ser. B Chem. Phys. Meteorol. 64 (1), 10925.

Cui, X.J., Wang, X.F., Yang, L.X., Chen, B., Chen, J.M., Andersson, A., Gustafsson, Ö., 2016. Radiative absorption enhancement from coatings on black carbon aerosols. Sci. Total Environ. 551, 51–56.

Dehkhoda, N., Noh, Y., Joo, S., 2020. Long-Term Variation of Black Carbon Absorption Aerosol Optical Depth from AERONET Data over East Asia. Remote Sens. 12 (21), 3551.

Deng, X.J., Tie, X.X., Zhou, X.J., Wu, D., Zhong, L.J., Tan, H.B., Li, F., Huang, X.Y., Bi, X. Y., Deng, T., 2008. Effects of Southeast Asia biomass burning on aerosols and ozone concentrations over the Pearl River Delta (PRD) region. Atmos. Environ. 42 (36), 8493–8501.

Drugé, T., Nabat, P., Mallet, M., Michou, M., Rémy, S., Dubovik, O., 2022. Modeling radiative and climatic effects of brown carbon aerosols with the ARPEGE-Climat global climate model. Atmos. Chem. Phys. 22 (18), 12167–12205.

Duc, H.N., Bang, H.Q., Quang, N.X., 2016. Modelling and prediction of air pollutant transport during the 2014 biomass burning and forest fires in peninsular Southeast Asia. Environ. Monit. Assess. 188 (2), 106.

Emery, C., Liu, Z., Russell, A.G., Odman, M.T., Yarwood, G., Kumar, N., 2017. Recommendations on statistics and benchmarks to assess photochemical model performance. J. Air Waste Manage. Assoc. 67 (5), 582–598.

Fan, Q., Wang, C.Z., Zhang, D.Y., Zang, S.Y., 2017. Environmental Influences on Forest Fire Regime in the Greater Hinggan Mountains, Northeast China. Forests 8 (10), 372.

Fan, W.X., Li, J., Han, Z.W., Wu, J., Zhang, S., Zhang, C.W., Li, J.W., 2023. Impacts of biomass burning in Southeast Asia on aerosols over the low-latitude plateau in China: an analysis of a typical pollution event. Front. Environ. Sci. 11, 1101745.

Feng, Y., Ramanathan, V., Kotamarthi, V.R., 2013. Brown carbon: a significant atmospheric absorber of solar radiation? Atmos. Chem. Phys. 13 (17), 8607–8621.

Feng, X., Wang, Jiandong, Teng, S., Xu, X., Zhu, B., Wang, Jiaping, Zhu, X., Yurkin, M.A., Liu, C., 2021. Can light absorption of black carbon still be enhanced by mixing with absorbing materials? Atmos. Environ. 253, 118358.

Fu, J.S., Hsu, N.C., Gao, Y., Huang, K., Li, C., Lin, N.H., Tsay, S.C., 2011. Evaluating the influences of biomass burning during 2006 BASE-ASIA: a regional chemical transport modeling. Atmos. Chem. Phys. 12 (9), 3837–3855.

Fu, T.M., Cao, J.J., Zhang, X.Y., Lee, S.C., Zhang, Q., Han, Y.M., Qu, W.J., Han, Z., Zhang, R., Wang, Y.X., Chen, D., Henze, D.K., 2012. Carbonaceous aerosols in China: top-down constraints on primary sources and estimation of secondary contribution. Atmos. Chem. Phys. 12 (5), 2725–2746.

Fu, J., Song, S.T., Guo, L., Chen, W.W., Wang, P., Duanmu, L.J., Shang, Y.J., Shi, B., He, L.Y., 2022. Interprovincial Joint Prevention and Control of Open Straw burning in Northeast China: Implications for Atmospheric Environment Management. Remote Sens. 14 (11), 2528.

Gelaro, R., McCarty, W., Suárez, M.J., Todling, R., Molod, A., Takacs, L., Randles, C.A., Darmenov, A., Bosilovich, M.G., Reichle, R., Wargan, K., Coy, L., Cullather, R., Draper, C., Akella, S., Buchard, V., Conaty, A., Da Silva, A.M., Gu, W., Kim, G.-K., Koster, R., Lucchesi, R., Merkova, D., Nielsen, J.E., Partyka, G., Pawson, S., Putman, W., Rienecker, M., Schubert, S.D., Sienkiewicz, M., Zhao, B., 2017. The Modern-Era Retrospective Analysis for Research and applications, Version 2 (MERRA-2). J. Clim. 30 (14), 5419–5454.

Guenther, A.B., Jiang, X., Heald, C.L., Sakulyanontvittaya, T., Duhl, T., Emmons, L.K., Wang, X., 2012. The Model of Emissions of gases and Aerosols from Nature version 2.1 (MEGAN2.1): an extended and updated framework for modeling biogenic emissions. Geosci. Model Dev. 5 (6), 1471–1492.

He, C.L., 2019. In: Springer Series in Light Scattering.

He, C.L., Liou, K.N., Takano, Y., Zhang, R., Levy Zamora, M., Yang, P., Li, Q., Leung, L.R., 2015. Variation of the radiative properties during black carbon aging: theoretical and experimental intercomparison. Atmos. Chem. Phys. 15 (20), 11967–11980.

He, C.L., Li, Q.B., Liou, K.N., Qi, L., Tao, S., Schwarz, J.P., 2016. Microphysics-based black carbon aging in a global CTM: constraints from HIPPO observations and implications for global black carbon budget. Atmos. Chem. Phys. 16 (5), 3077–3098.

Hua, Y., Tang, L.L., Liu, D.T., Zhang, Y.J., Jiang, L., Yu, Y.Y., Fu, Y., Chen, C., Qin, W., 2017. Source apportionment of black carbon aerosol during straw-burning period in spring and summer in Nanjing. Environ. Sci. Technol. 40 (1), 147–155 (in Chinese).

Huang, L., Zhu, Y.H., Wang, Q., Zhu, A.S., Liu, Z.Y., Wang, Y.J., Allen, D.T., Li, L., 2021. Assessment of the effects of straw burning bans in China: Emissions, air quality, and health impacts. Sci. Total Environ. 789, 147935.

Huang, R.J., Yuan, W., Yang, L., Yang, H.N., Cao, W.J., Guo, J., Zhang, N.N., Zhu, C.S., Wu, Y.F., Zhang, R.J., 2022. Concentration, optical characteristics, and emission factors of brown carbon emitted by on-road vehicles. Sci. Total Environ. 810, 151307.

Ji, D.S., Li, L., Pang, B., Xue, P., Wang, L.L., Wu, Y.F., Zhang, H.L., Wang, Y.S., 2017. Characterization of black carbon in an urban-rural fringe area of Beijing. Environ. Pollut. 223, 524–534.

Ji, D.S., Li, J.W., Shen, G.F., He, J., Gao, W.K., Tao, J., Liu, Y., Tang, G.Q., Zeng, L.M., Zhang, R.J., Wang, Y.S., 2022. Environmental effects of China's coal ban policy: results from in situ observations and model analysis in a typical rural area of the Beijing-Tianjin-Hebei region, China. Atmos. Res. 268, 106015.

Jin, Q.F., Ma, X.Q., Wang, W.H., Yang, S.Y., Guo, F.T., 2017. Temporal and spatial variations of PM2.5 emissions from crop straw burning in eastern China during 2000—2014. Acta Scien. Circum. 37 (2), 460–468 (in Chinese).

Jo, D.S., Park, R.J., Lee, S., Kim, S.-W., Zhang, X., 2016. A global simulation of brown carbon: implications for photochemistry and direct radiative effect. Atmos. Chem. Phys. 16 (5), 3413–3432.

Lan, J., Yan, Y., Qiao, L.P., 2020. Experimental analysis on sources and pollution characteristics of black carbon in metropolitan areas. J. Harbin Inst. Technol. 52 (11), 53–62 (in Chinese).

Li, J., Chen, X.X., Dong, J.J., Cao, Y., Ding, F., 2023. Research on Carbon Component Pollution Characteristics of Fine Particle Matter in Urban Area of Nanjing City from 2016 to 2020. China Resources Comprehensive Utilization. 41 (12), 222–227 (in Chinese).

Li, K., Liao, H., Mao, Y.H., Ridley, D.A., 2016. Source sector and region contributions to concentration and direct radiative forcing of black carbon in China. Atmos. Environ. 124, 351–366.

Li, M.J., Fan, X.J., Zhu, M.B., Zou, C.L., Song, J.Z., Wei, S.Y., Jia, W.L., Peng, P.A., 2019. Abundance and Light Absorption Properties of Brown Carbon Emitted from Residential Coal Combustion in China. Environ. Sci. Technol. 53 (2), 595–603.

Li, W.J., Riemer, N., Xu, L., Wang, Y.Y., Adachi, K., Shi, Z.B., Zhang, D.Z., Zheng, Z.H., Laskin, A., 2024. Microphysical properties of atmospheric soot and organic particles: measurements, modeling, and impacts. Npj Clim. Atmospheric Sci. 7 (1), 65.

Lian, C.Q., Xiao, C.W., Feng, Z.M., 2022. Spatiotemporal Characteristics and Regional Variations of active fires in China since 2001. Remote Sens. 15 (1), 54.

Lin, G.X., Penner, J.E., Flanner, M.G., Sillman, S., Xu, L., Zhou, C., 2014. Radiative forcing of organic aerosol in the atmosphere and on snow: Effects of SOA and brown carbon. J. Geophys. Res. Atmos. 119 (12), 7453–7476.

Liu, L., Mishchenko, M., 2018. Scattering and Radiative Properties of Morphologically complex Carbonaceous Aerosols: a Systematic Modeling Study. Remote Sens. 10 (10), 1634.

Liu Jacob, D.J., Bey, I., Yantosca, R.M., Duncan, B.N., Sachse, G.W., H.Y, 2003. Transport pathways for Asian pollution outflow over the Pacific: Interannual and seasonal variations. J. Geophys. Res. Atmos. 108 (D20), 8786.

Liu, J.M., Bergin, M., Guo, H.Y., King, L.E., Kotra, N., Edgerton, E., Weber, R.J., 2013. Size-resolved measurements of brown carbon in water and methanol extracts and estimates of their contribution to ambient fine-particle light absorption. Atmos. Chem. Phys. 13 (24), 12389–12404.

Liu, M.X., Song, Y., Yao, H., Kang, Y.N., Li, M.M., Huang, X., Hu, M., 2015. Estimating emissions from agricultural fires in the North China Plain based on MODIS fire radiative power. Atmos. Environ. 112, 326–334.

Liu, F., Zhang, Q., Van Der, A., R.J., Zheng, B., Tong, D., Yan, L., Zheng, Y.X., He, K.B., 2016. Recent reduction in NO_x emissions over China: synthesis of satellite observations and emission inventories. Environ. Res. Lett. 11 (11), 114002.

Liu, Y., Yan, C.Q., Zheng, M., 2018a. Source apportionment of black carbon during winter in Beijing. Sci. Total Environ. 618, 531–541.

Liu, Z.R., Gao, W.K., Yu, Y.C., Hu, B., Xin, J.Y., Sun, Y., Wang, L.L., Wang, G.H., Bi, X.H., Zhang, G.H., Xu, H.H., Cong, Z.Y., He, J., Xu, J.S., Wang, Y.S., 2018b. Characteristics of PM2.5 mass concentrations and chemical species in urban and background areas of China: emerging results from the CARE-China network. Atmos. Chem. Phys 18 (12), 8849–8871.

Liu, D.T., He, C.L., Schwarz, J.P., Wang, X., 2020a. Lifecycle of light-absorbing carbonaceous aerosols in the atmosphere. Npj Clim. Atmos. Sci. 3 (1), 40.

Liu, F.S., Yon, J., Fuentes, A., Lobo, P., Smallwood, G.J., Corbin, J.C., 2020b. Review of recent literature on the light absorption properties of black carbon: Refractive index,

mass absorption cross section, and absorption function. Aerosol Sci. Technol. 54 (1), 33–51.
Liu, Y.W., Wang, M.H., Qian, Y., Ding, A.J., 2022. A strong Anthropogenic Black Carbon Forcing Constrained by Pollution Trends over China. Geophys. Res. Lett. 49 (10), e2022GL098965.
Luo, J., Zhang, Q.X., Luo, J.F., Liu, J., Huo, Y.N., Zhang, Y.M., 2019. Optical Modeling of Black Carbon with Different Coating Materials: the effect of Coating Configurations. J. Geophys. Res. Atmos. 124 (23), 13230–13253.
Luo, J., Li, Z.Q., Zhang, C.C., Zhang, Q.X., Zhang, Y.M., Zhang, Y., Curci, G., Chakrabarty, R.K., 2022. Regional impacts of black carbon morphologies on shortwave aerosol–radiation interactions: a comparative study between the US and China. Atmos. Chem. Phys. 22 (11), 7647–7666.
Ma, X.Y., Yu, F.Q., Luo, G., 2012. Aerosol direct radiative forcing based on GEOS-Chem-APM and uncertainties. Atmos. Chem. Phys. 12 (12), 5563–5581.
Ma, G.X., Zhao, T.L., Kong, S.F., Bao, Y.S., Chen, C., Gong, S.L., Guo, J.P., Yu, C., Wu, M., Chang, J.C., You, Y.C., 2018. Variations in FINN Emissions of Particulate matters and Associated Carbonaceous Aerosols from Remote Sensing of Open Biomass burning over Northeast China during 2002–2016. Sustainability. 10 (9), 3353.
Mao, Y.H., Liao, H., Han, Y.M., Cao, J.J., 2016. Impacts of meteorological parameters and emissions on decadal and interannual variations of black carbon in China for 1980-2010: Black Carbon in China for 1980-2010. J. Geophys. Res. Atmos. 121 (4), 1822–1843.
Mao, Y.H., Zhao, X.C., Liao, H., Zhao, D.L., Tian, P., Henze, D.K., Cao, H.S., Zhang, L., Li, J.D., Li, J., Ran, L., Zhang, Q., 2020. Sources of black carbon during severe haze events in the Beijing–Tianjin–Hebei region using the adjoint method. Sci. Total Environ. 740, 140149.
Martinsson, J., Eriksson, A.C., Nielsen, I.E., Malmborg, V.B., Ahlberg, E., Andersen, C., Lindgren, R., Nyström, R., Nordin, E.Z., Brune, W.H., Svenningsson, B., Swietlicki, E., Boman, C., Pagels, J.H., 2015. Impacts of Combustion Conditions and Photochemical Processing on the Light Absorption of Biomass Combustion Aerosol. Environ. Sci. Technol. 49 (24), 14663–14671.
Meng, D.Y., Cao, F., Zhai, X.Y., Zhang, S.C., Zhang, Y.L., 2020. Effect of biomass burning on the light absorption properties of water-soluble organic carbon in atmospheric particulate matter in Changchun. Huan Jing Ke. Xue 41 (6), 2547–2554.
Meng, W.J., Zhong, Q.R., Chen, Y.L., Shen, H.Z., Yun, X., Smith, K.R., Li, B.G., Liu, J.F., Wang, X.L., Ma, J.M., Cheng, H.F., Zeng, E.Y., Guan, D.B., Russell, A.G., Tao, S., 2019. Energy and air pollution benefits of household fuel policies in northern China. Proc. Natl. Acad. Sci. 116 (34), 16773–16780.
Miao, R.Q., Chen, Q., Zheng, Y., Cheng, X., Sun, Y.L., Palmer, P.I., Shrivastava, M., Guo, J.P., Zhang, Q., Liu, Y.H., Tan, Z.F., Ma, X.F., Chen, S.Y., Zeng, L.M., Lu, K.D., Zhang, Y.H., 2020. Model bias in simulating major chemical components of PM2.5 in China. Atmos. Chem. Phys. 20 (20), 12265–12284.
Miao, R.Q., Chen, Q., Shrivastava, M., Chen, Y.F., Zhang, L., Hu, J.L., Zheng, Y., Liao, K. R., 2021. Process-based and observation-constrained SOA simulations in China: the role of semivolatile and intermediate-volatility organic compounds and OH levels. Atmos. Chem. Phys. 21 (21), 16183–16201.
Mo, Y.Z., Li, J., Cheng, Z.N., Zhong, G.C., Zhu, S.Y., Tian, C.G., Chen, Y.J., Zhang, G., 2021. Dual Carbon Isotope-based Source Apportionment and Light Absorption Properties of Water-Soluble Organic Carbon in $PM_{2.5}$ over China. J. Geophys. Res. Atmos. 126 (8), e2020JD033920.
Ni, H.Y., Huang, R.J., Pieber, S.M., Corbin, J.C., Stefenelli, G., Pospisilova, V., Klein, F., Gysel-Beer, M., Yang, L., Baltensperger, U., Haddad, I.E., Slowik, J.G., Cao, J.J., Prévôt, A.S.H., Dusek, U., 2021. Brown Carbon in primary and Aged Coal Combustion Emission. Environ. Sci. Technol. 55 (9), 5701–5710.
Novakov, T., Andreae, M.O., Gabriel, R., Kirchstetter, T.W., Mayol-Bracero, O.L., Ramanathan, V., 2000. Origin of carbonaceous aerosols over the tropical Indian Ocean: Biomass burning or fossil fuels? Geophys. Res. Lett. 27 (24), 4061–4064.
Park D.J., Chin, M., Martin, R,V., R.J. Jacob, 2003. Sources of carbonaceous aerosols over the United States and implications for natural visibility. J. Geophys. Res. Atmos. 108 (D12), 4355.
Park D.J., Palmer, P.I., Clarke, A.D., Weber, R., Zondlo, M.A., Eisele, F., Bandy, A.R., Thornton, D.C., Sachse, G.W., Bond, T.C., R.J., Jacob, 2005. Export efficiency of black carbon aerosol in continental outflow: Global implications. J. Geophys. Res. Atmos. 110 (D11), D11205.
Park, R.J., Kim, M.J., Jeong, J.I., Youn, D., Kim, S., 2010. A contribution of brown carbon aerosol to the aerosol light absorption and its radiative forcing in East Asia. Atmos. Environ. 44 (11), 1414–1421.
Patterson, E.M., McMahon, C.K., 1984. Absorption characteristics of forest fire particulate matter. Atmos. Environ. 18 (11), 2541–2551.
Peng, J.F., Hu, M., Guo, S., Du, Z.F., Zheng, J, Shang, D.J., Levy Zamora, M., Zeng, L.M., Shao, M., Wu, Y.S., Zheng, J., Wang, Y., Glen, C.R., Collins, D.R., Molina, M.J., Zhang, R.Y., 2016. Markedly enhanced absorption and direct radiative forcing of black carbon under polluted urban environments. Proc. Natl. Acad. Sci. 113 (16), 4266–4271.
Reddy, C.S., Unnikrishnan, A., Bird, N.G., Faseela, V.S., Asra, M., Manikandan, T.M., Rao, P.V.N., 2020. Characterizing Vegetation Fire dynamics in Myanmar and South Asian Countries. J. Indian Soc. Remote Sens. 48 (12), 1829–1843.
Saleh, R., 2020. From Measurements to Models: toward Accurate Representation of Brown Carbon in climate Calculations. Curr. Pollut. Rep. 6 (2), 90–104.
Saleh, R., Hennigan, C.J., McMeeking, G.R., Chuang, W.K., Robinson, E.S., Coe, H., Donahue, N.M., Robinson, A.L., 2013. Absorptivity of brown carbon in fresh and photo-chemically aged biomass-burning emissions. Atmos. Chem. Phys. 13 (15), 7683–7693.
Saleh, R., Robinson, E.S., Tkacik, D.S., Ahern, A.T., Liu, S., Aiken, A.C., Sullivan, R.C., Presto, A.A., Dubey, M.K., Yokelson, R.J., Donahue, N.M., Robinson, A.L., 2014. Brownness of organics in aerosols from biomass burning linked to their black carbon content. Nat. Geosci. 7 (9), 647–650.
Saleh, R., Marks, M., Heo, J., Adams, P.J., Donahue, N.M., Robinson, A.L., 2015. Contribution of brown carbon and lensing to the direct radiative effect of carbonaceous aerosols from biomass and biofuel burning emissions. J. Geophys. Res. Atmos. 120 (59), 10285–10296.
San, M., Xu, X.F., Dong, Y.L., Yu, X.M., Yue, Y., 2020. Observational Study of Black Carbon Aerosol Concentration at Atmospheric Background Station in Lin'an Region. J. Zhejiang Meteor. 41 (04), 25–29 (in Chinese).
Sand, M., Samset, B.H., Myhre, G., Gliß, J., Bauer, S.E., Bian, H., Chin, M., Checa-Garcia, R., Ginoux, P., Kipling, Z., Kirkevåg, A., Kokkola, H., Le Sager, P., Lund, M.T., Matsui, H., van Noije, T., Olivié, D.J.L., Remy, S., Schulz, M., Stier, P., Stjern, C.W., Takemura, T., Tsigaridis, K., Tsyro, S.G., Watson-Parris, D., 2021. Aerosol absorption in global models from AeroCom phase III. Atmos. Chem. Phys. 21 (20), 15929–15947.
Schnaiter Linke, C., Möhler, O., Naumann, K.H. Saathoff, H., Wagner, R., Schurath, U., M., 2005. Absorption amplification of black carbon internally mixed with secondary organic aerosol. J. Geophys. Res. Atmos. 110 (D19), D19204.
Shen, G.F., Tao, S., Wei, S., Chen, Y.C., Zhang, Y.Y., Shen, H.Z., Huang, Y., Zhu, D., Yuan, C.Y., Wang, H.C., Wang, Y.F., Pei, L.J., Liao, Y.L., Duan, Y.H., Wang, B., Wang, R., Lv, Y., Li, W., Wang, X.L., Zheng, X.Y., 2013. Field Measurement of Emission Factors of PM, EC, OC, Parent, Nitro-, and Oxy- Polycyclic Aromatic Hydrocarbons for Residential Briquette, Coal Cake, and Wood in Rural Shanxi, China. Environ. Sci. Technol. 47 (6), 2998–3005.
Shin, S.K., Tesche, M., Müller, D., Noh, Y., 2019. Technical note: Absorption aerosol optical depth components from AERONET observations of mixed dust plumes. Atmos. Meas. Tech. 12 (1), 607–618.
Sun, J.Z., Zhang, Y.Z., Zhi, G.R., Hitzenberger, R., Jin, W.J., Chen, Y.J., Wang, L., Tian, C. G., Li, Z.Y., Chen, R., Xiao, W., Cheng, Y., Yang, W., Yao, L.Y., Cao, Y., Huang, D., Qiu, Y.Y., Xu, J.L., Xia, X.F., Yang, X., Zhang, X., Zong, Z., Song, Y.C., Wu, C.D., 2021. Brown carbon's emission factors and optical characteristics in household biomass burning: developing a novel algorithm for estimating the contribution of brown carbon. Atmos. Chem. Phys. 21 (4), 2329–2341.
Tan, T.Y., Guo, S., Wu, Z.J., He, L.Y., Huang, X.F., Hu, M., 2020. Impact of aging process on atmospheric black carbon aerosol properties and climate effects. Chin. Sci. Bull. 65 (36), 4235–4250 (in Chinese).
Tang, L.Q., Hu, B., Liu, H., Zhao, S.M., Liu, J.Q., 2021. Aerosol optical properties and direct radiative forcing in Beijing in the recent decade. Climatic Environ. Res. 26 (2), 155–168 (in Chinese).
Tang, R., Huang, X., Zhou, D.R., Ding, A.J., 2020a. Biomass-burning-induced surface darkening and its impact on regional meteorology in eastern China. Atmos. Chem. Phys. 20 (10), 6177–6191.
Tang, J., Li, J., Su, T., Han, Y., Mo, Y.Z., Jiang, H.X., Cui, M., Jiang, B., Chen, Y.J., Tang, J.H., Song, J.Z., Peng, P.A., Zhang, G., 2020b. Molecular compositions and optical properties of dissolved brown carbon in biomass burning, coal combustion, and vehicle emission aerosols illuminated by excitation–emission matrix spectroscopy and Fourier transform ion cyclotron resonance mass spectrometry analysis. Atmos. Chem. Phys. 20 (4), 2513–2532.
Tian, X.R., Zhao, F.J., Shu, L.F., Wang, M.Y., 2013. Distribution characteristics and the influence factors of forest fires in China. For. Ecol. Manag. 310, 460–467.
Tian, J., Ni, H.Y., Cao, J.Y., Han, Y.M., Wang, Q.Y., Wang, X.L., Chen, L.-W.Antony, Chow, J.C., Watson, J.G., Wei, C., Sun, J., Zhang, T., Huang, R., 2017. Characteristics of carbonaceous particles from residential coal combustion and agricultural biomass burning in China. Atmos. Pollut. Res. 8 (3), 521–527.
Tuccella, P., Curci, G., Pitari, G., Lee, S., Jo, D.S., 2020. Direct Radiative effect of Absorbing Aerosols: Sensitivity to Mixing State, Brown Carbon, and Soil Dust Refractive Index and Shape. J. Geophys. Res. Atmos. 125 (2) e2019JD030967.
van der Werf, G.R., Randerson, J.T., Giglio, L., van Leeuwen, T.T., Chen, Y., Rogers, B.M., Mu, M., van Marle, M.J.E., Morton, D.C., Collatz, G.J., Yokelson, R.J., Kasibhatla, P. S., 2017. Global fire emissions estimates during 1997–2016. Earth Syst. Sci. Data 9 (2), 697–720.
Walcek, C.J., Brost, R.A., Chang, J.S., Wesely, M.L., 1986. SO2, sulfate and HNO3 deposition velocities computed using regional landuse and meteorological data. Atmos. Environ. 20 (5), 949–964.
Wang, Q.Q., Jacob, D.J., Fisher, J.A., Mao, J.Q., Leibensperger, E.M., Carouge, C.C., Le Sager, P., Kondo, Y., Jimenez, J.L., Cubison, M.J., Doherty, S.J., 2011. Sources of carbonaceous aerosols and deposited black carbon in the Arctic in winter-spring: implications for radiative forcing. Atmos. Chem. Phys. 11 (23), 12453–12473.
Wang, R., Tao, S., Wang, W.T., Liu, J.F., Shen, H.Z., Shen, G.F., Wang, B., Liu, X.P., Li, W., Huang, Y., Zhang, Y.Y., Lu, Y., Chen, H., Chen, Y.C., Wang, C., Zhu, D., Wang, X.L., Li, B.G., Liu, W.X., Ma, J.M., 2012. Black Carbon Emissions in China from 1949 to 2050. Environ. Sci. Technol. 46 (14), 7595–7603.
Wang, X., Heald, C.L., Ridley, D.A., Schwarz, J.P., Spackman, J.R., Perring, A.E., Coe, H., Liu, D., Clarke, A.D., 2014. Exploiting simultaneous observational constraints on mass and absorption to estimate the global direct radiative forcing of black carbon and brown carbon. Atmos. Chem. Phys. 14 (20), 10989–11010.
Wang, X., Heald, C.L., Sedlacek, A.J., De Sá, S.S., Martin, S.T., Alexander, M.L., Watson, T.B., Aiken, A.C., Springston, S.R., Artaxo, P., 2016. Deriving brown carbon from multiwavelength absorption measurements: methodand application to AERONET and Aethalometer observations. Atmos. Chem. Phys. 16 (19), 12733–12752.
Wang, X., Heald, C.L., Liu, J.M., Weber, R.J., Campuzano-Jost, P., Jimenez, J.L., Schwarz, J.P., Perring, A.E., 2018a. Exploring the observational constraints on the simulation of brown carbon. Atmos. Chem. Phys. 18 (2), 635–653.
Wang, H.B., Tian, M., Chen, Y., Shi, G.M., Liu, Y., Yang, F.M., Zhang, L.M., Deng, L.Q., Yu, J.Y., Peng, C., Cao, X.Y., 2018b. Seasonal characteristics, formation mechanisms

and source origins of PM2.5 in two megacities in Sichuan Basin, China. Atmos. Chem. Phys 18 (2), 865–881.
Wang, Q.Y., Ye, J.H., Wang, Y.C., Zhang, T., Ran, W.K., Wu, Y.F., Tian, J., Li, L., Zhou, Y. Q., Hang Ho, S.S., Dang, B., Zhang, Q., Zhang, R.J., Chen, Y., Zhu, C.S., Cao, J.J., 2019. Wintertime Optical Properties of primary and secondary Brown Carbon at a Regional Site in the North China Plain. Environ. Sci. Technol. 53 (21), 12389–12397.
Wang, Y.L., Wang, Y.S., Song, S.Y., Wang, T., Li, D., Tan, H.Z., 2020. Effects of coal types and combustion conditions on carbonaceous aerosols in flue gas and their light absorption properties. Fuel. 277 (D14), 118148.
Wang, Q.Q., Zhou, Y.Y., Ma, N., Zhu, Y., Zhao, X.C., Zhu, S.W., Tao, J.C., Hong, J., Wu, W.J., Cheng, Y.F., Su, H., 2022a. Review of Brown Carbon Aerosols in China: Pollution Level, Optical Properties, and Emissions. J. Geophys. Res. Atmos. 127 (16), e2021JD035473.
Wang, S., Feng, H.H., Zou, B., Yang, Z.L., Ding, Y., 2022b. Correlation between biomass burning and air pollution in China: Spatial heterogeneity and corresponding factors. Glob. Planet. Change. 213 (11), 103823.
Xie, M.J., Hays, M.D., Holder, A.L., 2017. Light-absorbing organic carbon from prescribed and laboratory biomass burning and gasoline vehicle emissions. Sci. Rep. 7 (1), 7318.
Xie, M.J., Shen, G.F., Holder, A.L., Hays, M.D., Jetter, J.J., 2018. Light absorption of organic carbon emitted from burning wood, charcoal, and kerosene in household cookstoves. Environ. Pollut. 240, 60–67.
Xie, X.C., Chen, Y.F., Nie, D.Y., Liu, Y., Liu, Y., Lei, R.Y., Zhao, X.Y., Li, H.W., Ge, X.L., 2020. Light-absorbing and fluorescent properties of atmospheric brown carbon: a case study in Nanjing, China. Chemosphere. 251 (56), 126350.
Xie, M.J., Lu, X.Y., Ding, F., Cui, W.N., Zhang, Y.Y., Feng, W., 2022. Evaluating the influence of constant source profile presumption on PMF analysis of PM2.5 by comparing long- and short-term hourly observation-based modeling. Environ. Pollut. 314, 120273.
Xu, J., 2020. Observational Study and Source Analysis of Black Carbon Aerosol in Dalian City. J. Hebei Univ. Environ. Eng. 30 (03), 51–55 (in Chinese).
Xu, Y.Q, Huang, Z.J., Jia, G.L., Fan, M., Cheng, L.X., Chen, L.F., Shao, M., Zheng, J.Y., 2019. Regional discrepancies in spatiotemporal variations and driving forces of open crop residue burning emissions in China. Sci. Total Environ. 671 (5), 536–547.
Yan, C.Q., Zheng, M., Bosch, C., Andersson, A., Desyaterik, Y., Sullivan, A.P., Collett, J.L., Zhao, B., Wang, S.X., He, K.B., Gustafsson, Ö., 2017. Important fossil source contribution to brown carbon in Beijing during winter. Sci. Rep. 7 (1), 43182.
Yan, J.P., Wang, X.P., Gong, P., Wang, C.F., Cong, Z.Y., 2018. Review of brown carbon aerosols: recent progress and perspectives. Sci. Total Environ. 634, 1475–1485.
Yang, Y., Wang, H.L., Smith, S.J., Ma, P.-L., Rasch, P.J., 2017. Source attribution of black carbon and its direct radiative forcing in China. Atmos. Chem. Phys. 17 (6), 4319–4336.
Yang, G.Y., Zhao, H.M., Tong, D.Q., Xiu, A.J., Zhang, X.L., Gao, C., 2020. Impacts of post-harvest open biomass burning and burning ban policy on severe haze in the Northeastern China. Sci. Total Environ. 716, 136517.
Yin, L.F., Du, P., Zhang, M.S., Liu, M.X., Xu, T.T., Song, Y., 2019. Estimation of emissions from biomass burning in China (2003–2017) based on MODIS fire radiative energy data. Biogeosciences 16 (7), 1629–1640.
Yu, Y.Y., Ding, F., Mu, Y.F., Xie, M.J., Wang, Q.G., 2020. High time-resolved PM2.5 composition and sources at an urban site in Yangtze River Delta, China after the implementation of the APPCAP. Chemosphere. 261, 127746.
Yuan, M.N., Wang, Q.Y., Zhao, Z.Z., Zhang, Y., Lin, Y., Wang, X.L., Chow, J.C., Watson, J. G., Tian, R.X., Liu, H.K., Tian, J., Cao, J.J., 2022. Seasonal variation of optical properties and source apportionment of black and brown carbon in Xi'an, China. Atmos. Pollut. Res. 13 (6), 101448.
Zhai, X.Y., Cao, F., Zhang, S.C., Yang, X.Y., Zhang, Y.L., 2019. Contribution of biomass burning on light absorption property of water-soluble organic carbon in PM2.5 in Sanjiang Plain, Northeast China. Ecology and Environ. Sci. 28 (3), 523.
Zhang, R.Y., Khalizov, A.F., Pagels, J.H., Zhang, D., Xue, H.X., McMurry, P.H., 2008. Variability in morphology, hygroscopicity, and optical properties of soot aerosols during atmospheric processing. Proc. Natl. Acad. Sci. 105 (30), 10291–10296.
Zhang, J.L., Reid, J.S., Alfaro-Contreras, R., Xian, P., 2017. Has China been exporting less particulate air pollution over the past decade? Geophys. Res. Lett. 44 (6), 2941–2948.
Zhang, A.X., Wang, Y.H., Zhang, Y.Z., Weber, R.J., Song, Y.J., Ke, Z.M., Zou, Y.F., 2020a. Modeling the global radiative effect of brown carbon: a potentially larger heating source in the tropical free troposphere than black carbon. Atmos. Chem. Phys. 20 (4), 1901–1920.
Zhang, Y., Li, Z.Q., Chen, Y., De Leeuw, G., Zhang, C., Xie, Y.S., Li, K.T., 2020b. Improved inversion of aerosol components in the atmospheric column from remote sensing data. Atmos. Chem. Phys. 20 (21), 12795–12811.
Zhang, L., Luo, Z.H., Xiong, R., Liu, X.L., Li, Y.J., Du, W., Chen, Y.C., Pan, B., Cheng, H.F., Shen, G.F., Tao, S., 2021a. Mass Absorption Efficiency of Black Carbon from Residential Solid Fuel Combustion and its Association with Carbonaceous Fractions. Environ. Sci. Technol. 55 (15), 10662–10671.
Zhang, Y., Peng, Y.R., Song, W.H., Zhang, Y.L., Ponsawansong, P., Prapamontol, T., Wang, Y.X., 2021b. Contribution of brown carbon to the light absorption and radiative effect of carbonaceous aerosols from biomass burning emissions in Chiang Mai. Thailand. Atmos. Environ. 260, 118544.
Zhao, B., Jiang, J.H., Gu, Y., Diner, D., Worden, J., Liou, K.-N., Su, H., Xing, J., Garay, M. J., Huang, L., 2017. Decadal-scale trends in regional aerosol particle properties and their linkage to emission changes. Environ. Res. Lett. 12 (5), 054021.
Zheng, L.J., Wu, Y., 2021. Effects of primary particle size on light absorption enhancement of black carbon aerosols using the superposition T-matrix method. J. Quant. Spectrosc. Radiat. Transf. 258 (11), 107388.
Zheng, B., Tong, D., Li, M., Liu, F., Hong, C.P., Geng, G.N., Li, H., Li, X.Y., Peng, L.Q., Qi, J., Yan, L., Zhang, Y.X., Zhao, H.Y., Zheng, Y.X., He, K.B., Zhang, Q., 2018. Trends in China's anthropogenic emissions since 2010 as the consequence of clean air actions. Atmos. Chem. Phys. 18 (19), 14095–14111.
Zhi, G.R., Chen, Y.J., Feng, Y.L., Xiong, S.C., Li, J., Zhang, G., Sheng, G.Y., Fu, J.M., 2008. Emission Characteristics of Carbonaceous Particles from various Residential Coal-Stoves in China. Environ. Sci. Technol. 42 (9), 3310–3315.
Zhou, B.H., Cao, X., Zhang, R.R., Yang, Z.L., Wang, J., Feng, Q., Liu, W.X., Wang, Y., 2021. Study on the Characteristics and Influencing Factors of Black Carbon Aerosol Concentration in Baoji High-Tech Zone. Environ. Monit. China. 37 (05), 125–132 (in Chinese).
Zhu, J., Xia, X.G., Wang, J., Zhang, J.Q., Wiedinmyer, C., Fisher, J.A., Keller, C.A., 2017. Impact of Southeast Asian smoke on aerosol properties in Southwest China: first comparison of model simulations with satellite and ground observations. J. Geophys. Res. Atmos. 122 (7), 3904–3919.
Zhong, J., Zhai, C.Z., Yu Peng, C., Chen, L., J.Y., 2016. Concentration characteristics of black carbon aerosol and its impact factors in Chongqing core area. J. Environ. Eng. 10 (02), 805–810 (in Chinese).
Zhu, Q.Z., Liu, Y.Z., Jia, R., Hua, S., Shao, T.B., Wang, B., 2018. A numerical simulation study on the impact of smoke aerosols from Russian forest fires on the air pollution over Asia. Atmos. Environ. 182, 263–274.
Zhu, H., Zhang, Z., Yang, S., Zhu, Z.P., Zeng, A.C., Guo, F.T., 2023. Temporal and spatial distribution of forest fire and the dynamics of fire danger period in southern and northern China: a case study in Heilongjiang and Jiangxi provinces. J. Ecol. 42 (1), 198–207 (in Chinese).
Zhuang, B.L., Liu, Q., Wang, T.J., Yin, C.Q., Li, S., Xie, M., Jiang, F., Mao, H.T., 2013. Investigation on semi-direct and indirect climate effects of fossil fuel black carbon aerosol over China. Theor. Appl. Climatol. 114 (3), 651–672.